Molecular Therapy
Nucleic Acids
Original Article

Fusogenic peptide delivery of bioactive siRNAs targeting CSNK2A1 for treatment of ovarian cancer

Timothy Samec,[1,2] Kharimat Lora Alatise,[1,2] Jessica Boulos,[1] Serena Gilmore,[1] Anthony Hazelton,[1] Carleigh Coffin,[1] and Angela Alexander-Bryant[1]

[1]Nanobiotechnology Laboratory, Department of Bioengineering, Clemson University, 301 Rhodes Research Center, Clemson, SC 29634-0905, USA

Ovarian cancer has shown little improvement in survival among advanced-stage patients over the past decade. Current treatment strategies have been largely unsuccessful in treating advanced disease, with many patients experiencing systemic toxicity and drug-resistant metastatic cancer. This study evaluates novel fusogenic peptide carriers delivering short interfering RNA (siRNA) targeting casein kinase II, *CSNK2A1*, for reducing the aggressiveness of ovarian cancer. The peptides were designed to address two significant barriers to siRNA delivery: insufficient cellular uptake and endosomal entrapment. The three peptide variants developed, DIVA3, DIV3H, and DIV3W, were able to form monodisperse nanoparticle complexes with siRNA and protect siRNAs from serum and RNase degradation. Furthermore, DIV3W demonstrated optimal delivery of bioactive siRNAs into ovarian cancer cells with high cellular uptake efficiency and mediated up to 94% knockdown of *CSNK2A1* mRNA compared with non-targeting siRNAs, resulting in decreased cell migration and recolonization *in vitro*. Intratumoral delivery of DIV3W-siCSNK2A1 complexes to subcutaneous ovarian tumors resulted in reduced CSNK2A1 mRNA and CK2α protein expression after 48 h and reduced tumor growth and migration in a 2-week multi-dosing regimen. These results demonstrate the potential of the DIV3W peptide to deliver bioactive siRNAs and confirms the role of CSNK2A1 in cell-cell communication and proliferation in ovarian cancer.

INTRODUCTION

Epithelial ovarian cancer is the seventh most commonly diagnosed cancer among women in the United States and has the highest mortality among all gynecological cancers.[1] Ovarian cancer is often diagnosed in late stages with a low response to therapeutic interventions, and, in the past 10 years, the survival rate for advanced-stage patients has only increased by 1%.[2,3] Because over 90% of ovarian cancers are derived from epithelial cells, tumors are prone to rapid proliferation and spreading, causing both local and distant metastases within ascites fluid.[4] Approximately 80% of patients experience recurrence, multidrug resistance, or distant metastasis when treated for advanced-stage disease.[5] To improve patient outcomes, there is a need for more effective ovarian cancer treatment strategies delivered via robust, biocompatible, and reliable mechanisms.

Gene therapy through RNA interference (RNAi) has been extensively studied as a potential therapeutic intervention in many cancer types since its discovery in 1998.[6–9] Short hairpin RNA (shRNA) or short interfering RNA (siRNA) can be used as RNAi tools to degrade target messenger RNA strands.[10] RNAi technology has significant implications in cancer treatment through the silencing of proteins responsible for cancer cell survival, migration, invasion, regrowth, and development of multidrug resistance.[11] Although RNAi-based therapy is highly specific and has been shown to be advantageous in drug-resistant cancers, siRNA delivery can be difficult to achieve without a nanocarrier due to its size, negative charge, and rapid degradation within the endosome.[12–17]

Peptide-based systems have great promise for applications in RNAi therapy due to their ability to complex with and efficiently deliver siRNAs for sequence-specific mRNA degradation in cancer. Peptide carriers may provide a method of eluding barriers to siRNA delivery, including rapid RNase-induced degradation, inefficient cell uptake, and lack of endosomal escape.[6,18–20] More specifically, fusogenic peptide sequences have been shown to efficiently complex siRNAs through electrostatic interactions, mediate cellular uptake via endocytosis, and cause endosomal escape via membrane disruption.[6,21–24] Due to their amphipathic nature, fusogenic peptides are able to interact with the cell membrane via hydrophobic amino acid residue affinity for the lipid bilayer membrane, inducing endocytosis. When encapsulated in the endosome, fusogenic peptides undergo a pH-dependent conformational change, primarily forming an α-helical structure, though some β sheet formation has been recorded and reported to have similar fusion with the endosomal membrane.[17,25] The newly conformed peptide structure can then insert itself into the endosomal membrane via the projection of hydrophobic amino acid residues, resulting in membrane structure destabilization and breakdown, allowing for the internalized cargo to dissociate from the fusogenic peptide delivery system and escape into the cytosol (Figure 1).[17]

Received 10 November 2021; accepted 15 September 2022;
https://doi.org/10.1016/j.omtn.2022.09.012.

[2]These authors contributed equally

Correspondence: Angela Alexander-Bryant, Nanobiotechnology Laboratory, Department of Bioengineering, Clemson University, 301 Rhodes Research Center, Clemson, SC 29634-0905, USA.
E-mail: angelaa@clemson.edu

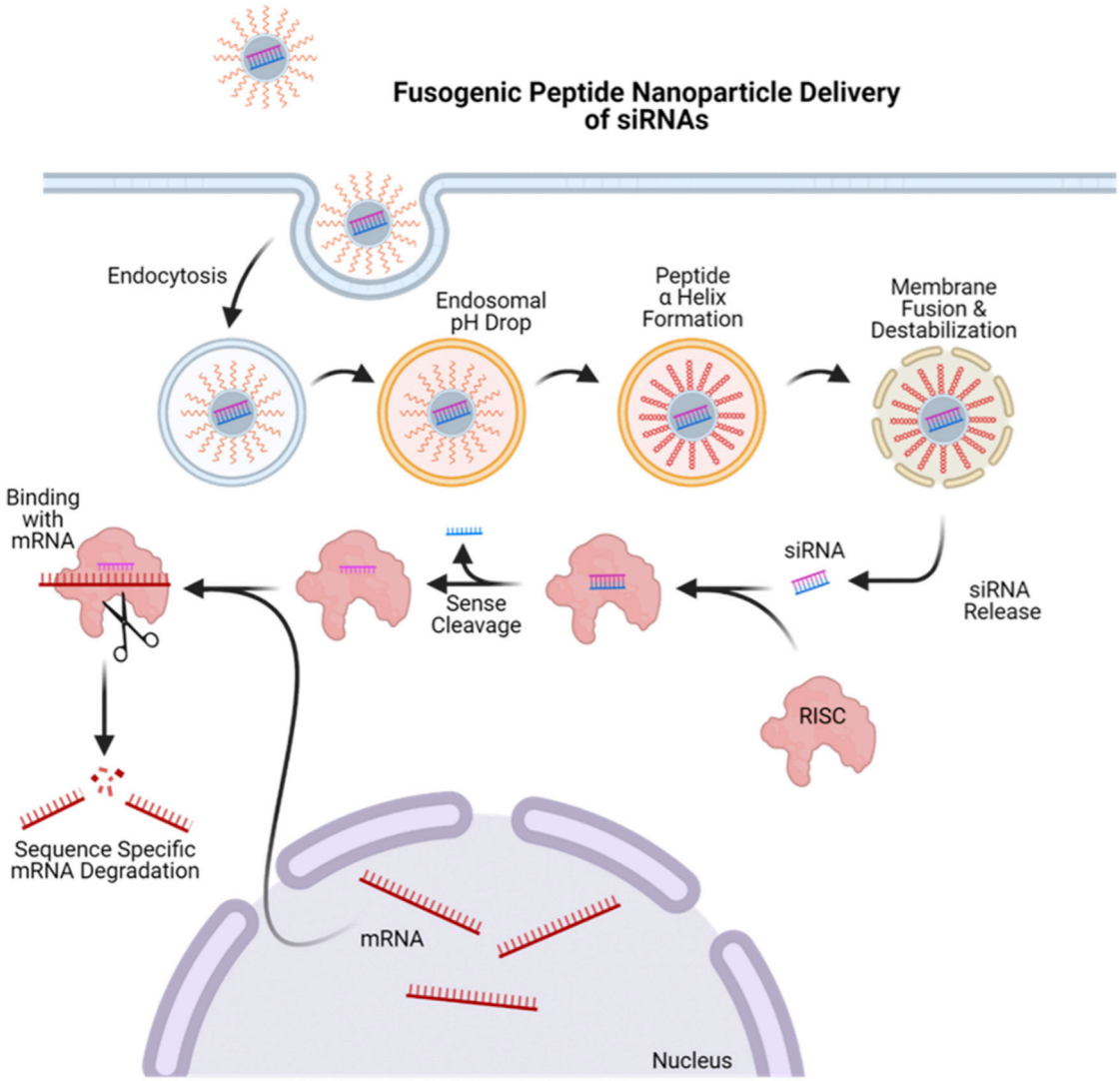

Figure 1. Fusogenic nanoparticle delivery and endosomal membrane fusion

Fusogenic peptides may address two primary barriers to siRNA therapeutic delivery in cancer through encouraging endocytosis and facilitating endosomal escape via pH-dependent protonation, conformational shift of the peptide, and insertion into the endosomal membrane. Upon membrane puncture, therapeutic cargo can dissociate from the peptide and escape into the cytosol for RNA-induced silencing complex formation and mRNA degradation.

We have developed a set of rationally designed fusogenic peptides for complexation with siRNAs to be delivered into genetically relevant epithelial ovarian cancer cell lines, OVCAR3 and CAOV3.[26] Each peptide was designed to maintain amphipathic properties and include a sequence of D-arginine residues responsible for siRNA complexation. In this study, we have demonstrated the ability of three fusogenic peptides to electrostatically bind with siRNAs, protect siRNA cargo from serum degradation, and encourage endosomal escape and delivery of bioactive siRNAs. Specifically, we examined the potential of *CSNK2A1* as a gene target in ovarian cancer via delivery of the novel fusogenic peptides complexed with siRNAs. *CSNK2A1* is an oncogene found overexpressed in several cancer types, including ovarian cancer, and is responsible for increased growth and cell survivability in the presence of chemotherapeutic agents.[27,28] The protein encoded by *CSNK2A1*, CK2α, plays a major role in cell cycle regulation, cell-cell communication, DNA repair activation, and apoptosis in response to external stimuli in lung adenocarcinoma, urothelial carcinoma, and pancreatic adenocarcinoma.[29,30] Roles in ovarian cancer, however, have only been suggested through observation of upregulation of CK2α and combination treatment with chemotherapeutics, including dasatinib, cisplatin, and gemcitabine.[31,32] RNAi-based therapies alone that target *CSNK2A1* have not been comprehensively studied; thus, this work assesses the therapeutic efficacy of siCSNK2A1 monotherapy in ovarian cancer delivered using novel fusogenic peptides.

Our results show that knockdown of CK2α protein using the DIV3W peptide complexed with siRNA targeting *CSNK2A1* decreased cell migration and invasion in ovarian cancer *in vitro* and *in vivo*. The DIV3W peptide encouraged high cellular uptake efficiency and significant gene and protein silencing, but cytotoxic effects from targeting *CSNK2A1* were not observed. Despite this, the reduction in cell migration and colonization demonstrates the therapeutic potential of *CSNK2A1* as a gene target to reduce ovarian cancer aggressiveness. Our *in vivo* data demonstrate that, when complexed to DIV3W, siRNA was localized to xenograft ovarian tumors, which resulted in reduced *CSNK2A1* mRNA expression and CK2α protein levels after single-dose and multi-dosing treatment. Additionally, intratumoral administration of DIV3W-siCSNK2A1 into subcutaneous (SQ) ovarian tumors led to tumor growth inhibition and reduced tumor volumes. These data demonstrate the potential of the DIV3W peptide as a delivery system for RNAi-based therapy.

RESULTS

Characterization of DIVA3, DIV3H, and DIV3W peptides

Peptides were systematically designed based on the prominent fusogenic peptide, GALA, a synthetic peptide derived from the viral fusion sequence of the HA2 protein found in the influenza virus.[33,34] Each amino acid was selected to formulate an amphipathic sequence repeat, consisting of hydrophilic and hydrophobic residues. The N terminus includes a nona-D-arginine sequence to enable electrostatic complexion with siRNAs, which is separated from the amphipathic, fusogenic sequence at the C terminus by a glycine linker. The three peptides, DIVA3, DIV3H, and DIV3W, were designed to follow these formulations, with an additional histidine residue and tryptophan residue present in DIV3H and DIV3W, respectively.

Agarose gel electrophoresis was used to determine the ability of DIVA3, DIV3H, and DIV3W (all three denoted as DIV3(X)) peptides to completely complex free siRNAs and protect siRNAs from degradation. The DIVA3 peptide was able to completely complex free siRNAs at the lowest molar ratio of positively charged amine content in the peptide to negatively charged phosphate content in the siRNA (N:P), at 20:1. In contrast, a minimum molar ratio of 40:1 was required for complete complexation of DIV3H and DIV3W with siRNAs (Figure 2A). To mimic physiological conditions and examine the ability of the peptides to protect siRNAs from degradation, DIV3(X) peptides were complexed with non-targeting siRNA (siNT) at several N:P ratios and exposed to 50% serum (Figure 2B) or RNase A (Figure 2C) for 1 h followed by agarose gel electrophoresis. White bands indicate intact siRNA and can be observed for DIV3W-siRNA complexes subjected to 50% serum at all N:P molar ratios. Reduction of intact siRNA signal was detected for DIVA3 and DIV3H complexes at 40:1 to 80:1 ratios incubated with 50% serum (Figure 2B) and at 20:1 and 80:1 molar ratios of the DIVA3 complexes when incubated with RNase A (Figure 2C). Minimal degradation, specifically in the DIV3W formulations after incubation in RNase A, indicates that the peptides protected siRNA from degradation (Figure 2C).

Peptide molar ratios of 40:1, 60:1, and 80:1 were selected for subsequent experiments following confirmation of full siRNA complexation at each of these ratios for all three peptide variants. Each peptide/siRNA complex was characterized by dynamic light scattering to determine the nanoparticle size distribution and surface charge to ensure stability (Figures 2D and 2E). All DIV3(X)-siRNA complexes formed positively charged, monodisperse nanoparticles that were within the appropriate size range advantageous for passive targeting through the enhanced permeability and retention effect.[35] DIV3W-siRNA and DIV3H-siRNA complexes were the largest, with a hydrodynamic diameter of 100.38 ± 3.59 nm and 98.66 ± 3.62 nm, respectively, while DIVA3 formed complexes sized 85.07 ± 3.15 nm (Figures 2D and 2E). Transmission electron microscopy (TEM) of DIV3W-siRNA complexes (Figure 2F) confirmed the formation of spherical nanoparticles.

DIV3(X) peptides exhibit biocompatibility with ovarian cancer cells

To evaluate the effect of the peptides on cell viability, OVCAR3 and CAOV3 cells were treated with DIV3(X) peptides alone at concentrations equivalent to 40:1, 60:1, and 80:1 molar ratios for each formulation. After a 48-h treatment, none of the peptide formulations demonstrated any significant cytotoxicity compared with untreated cells (Figure 3). To examine biocompatibility with healthy cells, DIV3W was treated for 48 h on MCF10a breast epithelial cells where no cytotoxic effects were observed (Figure S1). These results confirm the biocompatibility of the DIV3(X) peptides and their potential for *in vivo* evaluation.

DIV3(X) peptides enable siRNA uptake into ovarian cancer cells via endocytosis

A major barrier to siRNA delivery is inefficient cellular uptake. Through fluorescence microscopy and flow cytometry, we examined the ability of the DIV3(X) peptides to deliver fluorescently labeled siRNAs into ovarian cancer cells. Fluorescence microscopy revealed that uptake of DY547 fluorescently labeled non-targeting siRNA (siNT-DY547) into OVCAR3 and CAOV3 cells increased with increasing N:P ratios across each peptide variant. Furthermore, siNT-DY547 uptake into ovarian cancer cells also increased with the use of DIV3W compared with DIVA3 and DIV3H (Figures 4A and S2A). Qualitative observations of siRNA uptake were confirmed with flow cytometry, which also demonstrated increasing uptake efficiency with increasing N:P ratios (Figures 4B and S2B). N:P molar ratio-dependent increases in siRNA uptake were apparent for all formulations, except DIV3W, which displayed high levels of uptake across all N:P ratios in OVCAR3 cells (Figure 4C). DIV3W uptake efficiency was 70.0%, 69.7%, and 66.6% for 40:1, 60:1, and 80:1 molar ratios, respectively. DIV3H and DIVA3 peptides exhibited optimum cell uptake at an 80:1 ratio, at 52.1% and 63.6% efficiency, respectively (Figure 4C). In CAOV3 cells, no statistically significant results were found between peptide variants, but uptake did increase with higher N:P ratios (Figure S2C).

Another significant barrier to the delivery of endocytosed nanocarriers is endosomal entrapment, resulting in lysosomal trafficking and degradation of nanocarriers, inhibiting the bioactivity of the

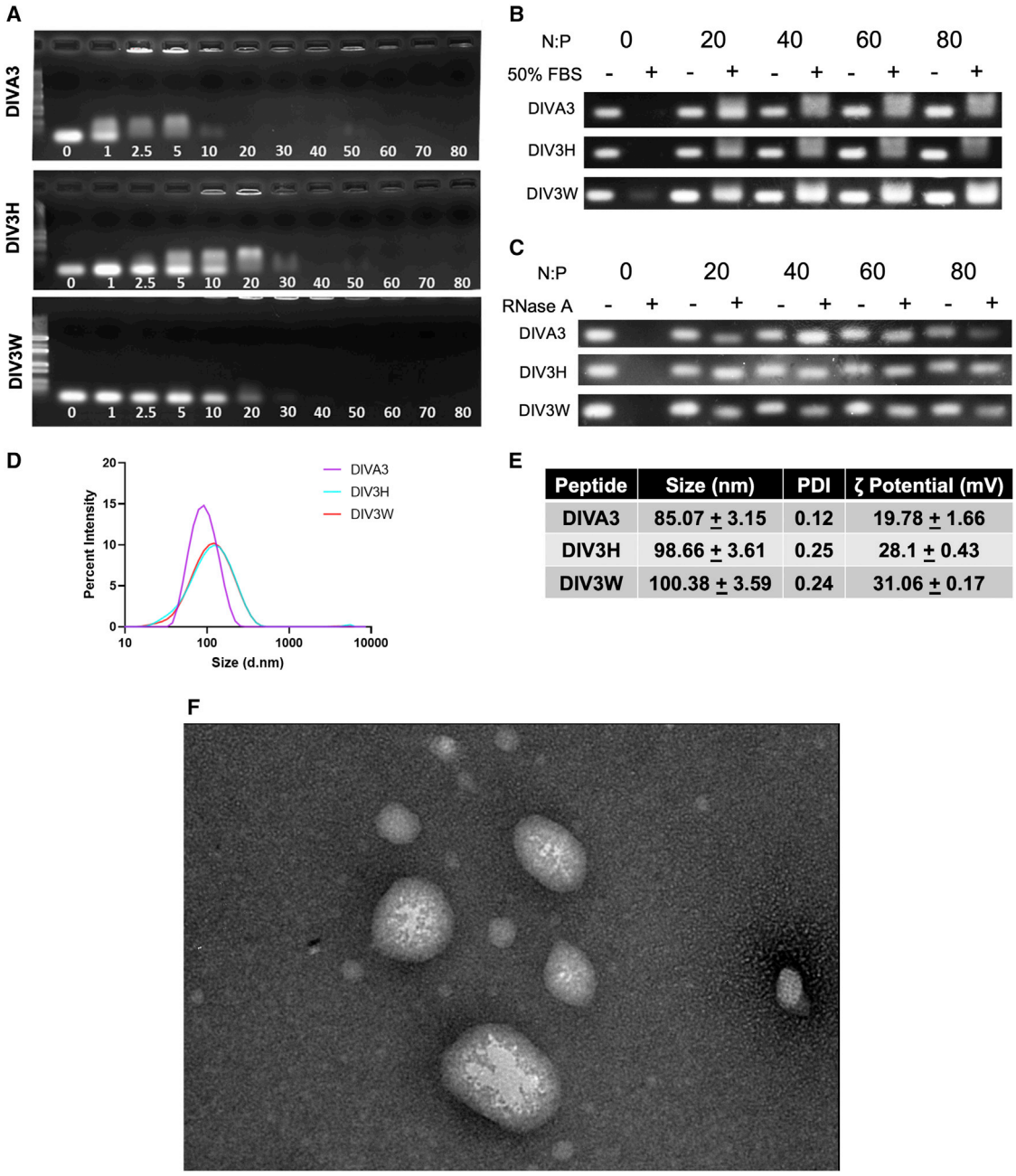

Peptide	Size (nm)	PDI	ζ Potential (mV)
DIVA3	85.07 ± 3.15	0.12	19.78 ± 1.66
DIV3H	98.66 ± 3.61	0.25	28.1 ± 0.43
DIV3W	100.38 ± 3.59	0.24	31.06 ± 0.17

Figure 2. Fusogenic peptide characterization

Peptides were electrostatically complexed with siRNAs at increasing N:P ratios and subjected to agarose gel electrophoresis (A) Peptide-siRNA complexes were incubated in 50% fetal bovine serum (FBS) (B) or RNase A (C) for 1 h, dissociated using SDS, and subjected to agarose gel electrophoresis. Size distribution (D), polydispersity index (PDI), and surface ζ-potential (E) were determined by dynamic light scattering and Doppler voltage velocities for each DIV3(X) peptide/siRNA complex at a 60:1 ratio. Data are mean ± SD performed in triplicate. TEM confirmed the size and morphology of DIV3W-siRNA complexes at a 60:1 ratio (F) Scale bar: 200 nm.

delivered siRNAs. The primary functional characteristic of the DIV3(X) fusogenic peptides is their ability to overcome this barrier by mediating endosomal escape through fusion of exposed hydrophobic amino acids with the endosomal membrane following protonation of anionic residues. Each DIV3(X) peptide was complexed with siNT-DY547 at a 60:1 molar ratio and incubated with OVCAR3 or CAOV3 cells for 4 h (Figure 5A) and 8 h (Figure 5B) prior to staining for early endosome antigen-1 (EEA1). Endosomal accumulation of siRNA indicates intracellular localization of the delivered complexes and was observed for all peptide complexes after 4 h. However, colocalized

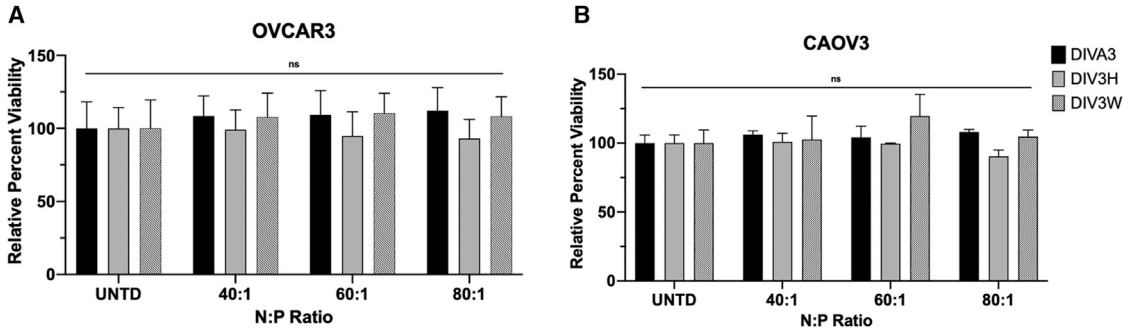

Figure 3. Fusogenic peptide biocompatibility via MTS assay

Cell viability after 48-h treatment with each peptide formulation using OVCAR3 (A) and CAOV3 (B) cells. Data are mean ± SEM of three independent experiments performed in triplicate and analyzed via one-way ANOVA. ns, not significant.

signal of siNT-DY547 and EEA1 stain decreased after allowing the complexes to incubate for 8 h before imaging, suggesting successful release of siRNA cargo from the endosome into the cytosol.

DIV3W-siCSNK2A1 complexes silence CSNK2A1 mRNA and CK2α protein expression in ovarian cancer cells

Confirmation of endosomal escape of siRNAs mediated by the DIV3(X) peptides was further confirmed through evaluation of siRNA bioactivity via gene silencing. Higher levels of gene silencing are associated with higher levels of cellular uptake, endosomal escape, and release of bioactive siRNAs. Gene silencing efficiency was determined by analyzing *CSNK2A1* mRNA and CK2α protein levels in ovarian cancer cells treated with DIV3(X) peptides complexed with siNT or siCSNK2A1 for 48 h. DIVA3 (Figure 6A) and DIV3H (Figure 6B) complexes mediated statistically significant reduction of *CSNK2A1* mRNA expression in OVCAR3 cells, but only at a 60:1 ratio in DIVA3 complexes and an 80:1 ratio in DIV3H complexes, at 47% and 72% silencing efficacy (Figures 6E and 6F). DIV3W-siCSNK2A1 complexes significantly reduced *CSNK2A1* mRNA expression in OVCAR3 cells compared with DIV3W-siNT by 95% and 65% at 60:1 and 80:1 molar ratios, respectively (Figure 6C). Significant reduction of *CSNK2A1* mRNA expression was also observed in CAOV3 cells when treated with DIV3W complexes at all N:P molar ratios, with a maximum of 80% knockdown using an 80:1 N:P ratio (Figure S3A). Due to their reduced silencing efficiency compared with DIV3W, DIVA3 and DIV3H were not included for protein analysis or CAOV3 qPCR studies. Western blot analysis revealed that expression of CK2α protein was silenced in OVCAR3 cells across all N:P ratios (Figure 6D) and CAOV3 cells at 40:1 and 80:1 ratios (Figure S3B) after treatment with DIV3W-siCSNK2A1 complexes compared with DIV3W-siNT. The significant *CSNK2A1* mRNA and CK2α protein knockdown mediated by DIV3W warrants the selection of this peptide for subsequent anticancer studies.

DIV3W peptide-mediated silencing of CSNK2A1 inhibits ovarian cancer cell migration and colonization

Analyzing the anticancer effect of silencing *CSNK2A1* mRNA and CK2α protein can provide support for utilizing *CSNK2A1* as a prospective therapeutic gene target for the treatment of ovarian cancer. Initial evaluation of the effect of *CSNK2A1* knockdown on ovarian cancer cell viability using an MTS [3-(4,5-dimethylthiazol-2-yl)-5-(3-carboxymethoxyphenyl)-2-(4-sulfophenyl)-2H-tetrazolium] assay did not produce statistically significant results (Figure S3A). To evaluate the effect of silencing *CSNK2A1* on cell migration, a scratch wound assay was conducted by first treating OVCAR3 cells with DIV3W-siNT or DIV3W-siCSNK2A1 complexes for 48 h. Following treatment, a vertical and horizontal scratch wound was introduced on the cell monolayer in each treatment group. Consistent with our uptake and knockdown studies, delivery of DIV3W-siCSNK2A1 complexes at the 40:1 N:P ratio did not exhibit significant inhibition of cell migration compared with treatment with siNT, with cell migration across the scratch area covering 88.8% ± 1.2% of the width in the siNT group and 63.7% ± 15.6% in the siCSNK2A1 group (Figures 7A and 7B). Although cells treated with the complexes at the 60:1 N:P ratio did demonstrate some inhibited wound recovery, with 24.7% ± 13.7% of the wound area being repopulated with cells in the siCSNK2A1 group, only the 80:1 ratio demonstrated a statistically significant reduction of migration, with only 9.9% ± 7.2% wound closure in siCSNK2A1-treated cells compared with 82.2% ± 14.7% closure in cells treated with siNT (Figures 7A and 7B). CAOV3 cells treated with DIV3W complexes at an 80:1 N:P ratio also displayed a significant reduction after 72 h, with siCSNK2A1 treatment reducing the scratch wound closure by 45.6% ± 11.9% compared with siNT (Figures S4B and S4C).

To determine the effect of *CSNK2A1* gene silencing on the long-term proliferative potential of ovarian cancer cells, a clonogenic assay was performed. Treatment of ovarian cancer cells with DIV3W-siNT complexes was compared with DIV3W-siCSNK2A1 complexes at an 80:1 N:P ratio (Figures 7C and 7D). OVCAR3 and CAOV3 cells both exhibited a statistically significant decrease in their ability to recolonize, with 78.5% ± 2.5% and 76.4% ± 4.3% relative colonization, respectively, when treated with siCSNK2A1 compared with siNT (Figure 7E). This reduction in cell migration and clonogenicity in both cell lines demonstrates the therapeutic potential of *CSNK2A1* as a gene target for ovarian cancer.

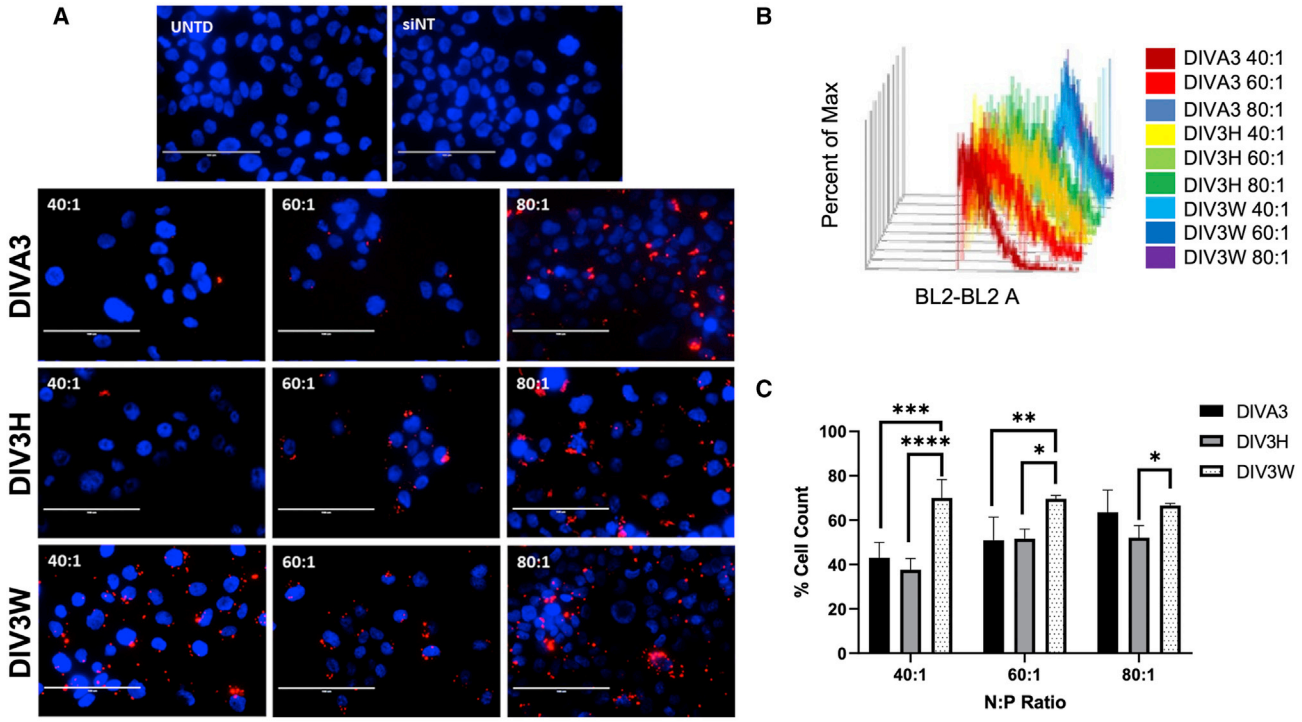

Figure 4. Fusogenic peptide uptake efficiency *in vitro* in OVCAR3 cells

(A) Fluorescence microscopy of siRNA uptake in OVCAR3 cells left untreated (UNTD), treated with siNT alone, or DIV3(X) peptide-siNT-DY547 (red) complexes for 4 h. Cells are counterstained with Hoechst 33342 (blue). Scale bar: 100 μm. Flow cytometric analysis (B) and cell count quantification (C) of DIV3(X)-siNT-DY547 uptake into OVCAR3 cells after 4 h. Data are mean ± SEM of three independent experiments analyzed with one-way ANOVA and *post hoc* Tukey multiple comparisons testing, where *$p \leq 0.05$, **$p \leq 0.01$, ***$p \leq 0.001$, and ****$p \leq 0.0001$.

DIV3W increases siRNA accumulation in SQ and intraperitoneal tumors following intratumoral or intraperitoneal administration

In vivo studies were conducted to evaluate the therapeutic potential of the DIV3W peptide for siRNA delivery. SQ and intraperitoneal (IP) models of ovarian cancer were generated in mice using OVCAR3 cells. To assess intratumoral accumulation of siRNA, mice were treated with either non-targeting siRNA fluorescently labeled with Cy5.5 (siNT-Cy5.5) or DIV3W complexed with siNT-Cy5.5 (DIV3W-siNT-Cy5.5). SQ and IP tumors were treated via intratumoral or IP injection, respectively. DIV3W-siNT-Cy5.5 complexes exhibited significantly enhanced tumor localization of Cy5.5-siNT signal compared with free siNT-Cy5.5 at all time points for SQ tumors with intratumoral delivery (Figures 8A and 8B). DIV3W-siNT-Cy5.5 complexes also exhibited higher fluorescence intensity in IP tumors via IP delivery after 24 h compared with siNT-Cy5.5 alone (Figures 9A and 9B); however, when quantified, these differences were not significant. Additionally, intratumoral injections of DIV3W-siNT-Cy5.5 in SQ tumors remained localized to the tumor compared with IP injection in the IP tumor model. IVIS imaging revealed differences in the localization of fluorescent signal, where focal distribution of siRNA was observed in SQ tumors that received intratumoral injections (Figure 8A), while regional fluorescence within the entire IP cavity was observed for IP tumors with IP treatment (Figure 9A). Overall, whole-animal imaging following both intratumoral and IP injection of DIV3W-siNT-Cy5.5 complexes exhibited higher fluorescence across the entire 24-h period compared with siNT-Cy5.5 alone, further demonstrating the ability of the DIV3W peptide to protect siRNAs from degradation. *Ex vivo* imaging of organs and tumors from the SQ group (Figure 8C) confirmed the higher fluorescence intensity of siNT-Cy5.5 in the tumor tissue compared with other tissues. In the IP group, fluorescent signal was not detected in the IP tumors treated with DIV3W-siCSNK2A1. Additionally, some fluorescent signal for siNT, in both SQ and IP tumors, was found in the liver, kidneys, and spleen (Figures 8C and 9C). Because siRNA accumulation was significantly increased in SQ models compared with IP models, subsequent gene silencing studies were conducted using SQ tumors with intratumoral administration of treatments.

DIV3W-mediated delivery of siCSNK2A1 causes silencing of *CSNK2A1* in SQ tumors after a single-dose treatment

To determine the ability of the DIV3W peptide to mediate delivery of bioactive siRNAs into ovarian tumor tissue, bioactivity was evaluated in SQ tumors 48 h post treatment with DIV3W-siCSNK2A1

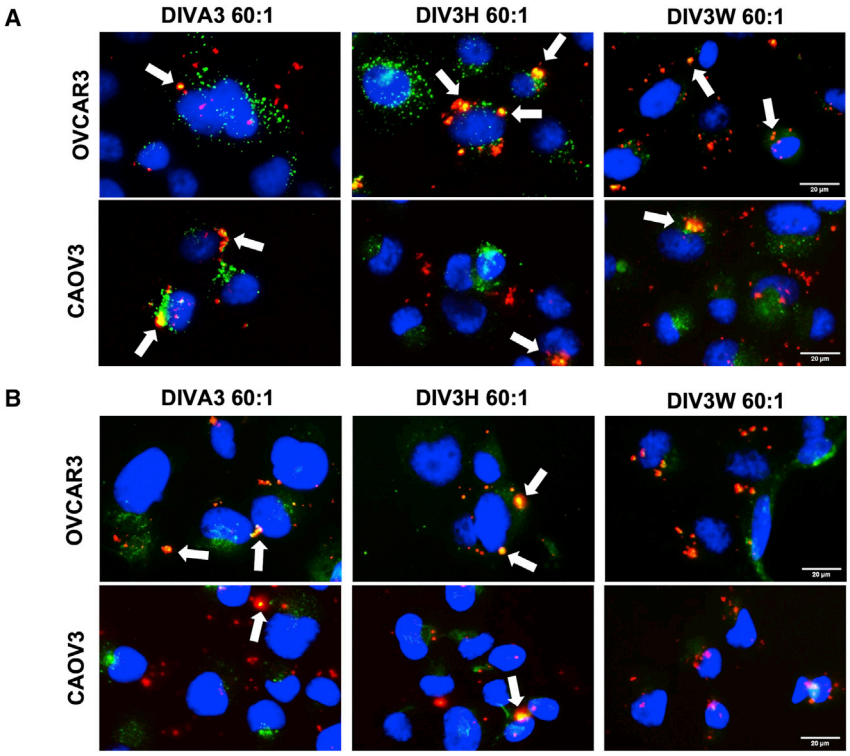

Figure 5. Endosomal escape ability of DIV3W

Immunofluorescence microscopy of early endosome antigen-1 (green) after incubation of OVCAR3 (A) and CAOV3 (B) cells with siNT-DY547 (red) complexed with DIV3(X) peptides at a 60:1 N:P ratio for 4 and 8 h. Colocalized green and red fluorescence (yellow) indicates endosomal entrapment of the peptide/siRNA complexes, identified with white arrows, while siRNA that has escaped can be seen in red in the overlay image. Cell nuclei are counterstained with Hoechst 33342 (blue). Scale bar: 20 μm.

complexes via intratumoral injection (Figure 10A). In a single dose of 0.5 mg/kg siRNA, DIV3W-siCSNK2A1 decreased expression of *CSNK2A1* mRNA to 22.53% ± 8.24% in SQ tumors (Figure 10B). DIV3W-siNT treatment had no significant effects on *CNSK2A1* gene expression (Figure 10B).

DIV3W-siCSNK2A1-mediated knockdown of CSNK2A1 reduces tumor burden in SQ tumors following a multi-dosing schedule

A multi-dosing study was completed to evaluate the efficacy of the DIV3W peptide delivery system and *CSNK2A1* as a therapeutic gene target. Mice with SQ flank ovarian tumors were intratumorally injected with saline, DIV3W-siNT, or DIV3W-siCSNK2A1 in four doses over a 2-week period. Excised tumors were evaluated for *CSNK2A1* mRNA (Figure 11A) and CK2α protein (Figure 11B) expression. qPCR analysis revealed that mice treated with DIV3W-siCSNK2A1 yielded only 37.7% ± 11.2% *CSNK2A1* mRNA expression relative to saline controls and 16.4% ± 11.2% mRNA expression compared with DIV3W-siNT-treated animals (Figure 11A). A reduction in CK2α protein production was also noted through western blotting (Figure 11B) and immunocytochemistry analysis of tumor tissue (Figure 11C). Analysis of tumor volume over time revealed that DIV3W-siCSNK2A1 treatments reduced the growth rate of treated tumors such that they were only 33.37 ± 26.68 mm^3 larger than the volume at the first treatment injection (Figure 12B). In contrast, DIV3W-siNT-treated tumors were 205.25 ± 25.77 mm^3 larger in volume, and saline-treated tumors grew 224.22 ± 78.51 mm^3 over the course of the study (Figure 12B). Final tumor masses and volumes were also recorded following tumor retrieval (Figures 12C and 12D). The mean volumes of resected tumors were 78.29 ± 18.07 mm^3, 266.74 ± 27.37 mm^3, and 270.67 ± 80.21 mm^3 for mice treated with DIV3W-siCSNK2A1, DIV3W-siNT, and saline, respectively. Additionally, vimentin and Akt mRNA levels were assessed to determine downstream effects on cellular migration, growth, and proliferation. In tumors treated with DIV3W-siCSNK2A1, vimentin and Akt mRNA levels were downregulated 2-fold; however, the differences were not statistically significant between the DIV3W-siCSNK2A1 treatment and saline or siNT controls (Figure 13).

DISCUSSION

Endosomal entrapment of nanocarriers encapsulating siRNA and activation of the lysosomal degradation pathway significantly hinders the translatability of siRNA therapies through acidic degradation.[36] Several nanoparticle systems are able to encapsulate and deliver siRNA to cancer cells but may have reduced biocompatibility and allow insufficient endosomal escape.[37–39] Cell-penetrating peptides cause endosomal escape via the proton sponge effect but have been shown to induce cytotoxic effects on cells because of their strong positive charge.[40] Conversely, lipid and polymer nanoparticles have high biocompatibility but may require the addition of cationic peptides or lipid/polymer formulation changes to increase the charge necessary for endosomal escape capabilities; however, these modifications can hinder uptake and increase cytotoxicity.[41–44] This work explores novel fusogenic peptides as a viable carrier for RNAi therapeutics that may overcome barriers of cellular uptake, biocompatibility, and endosomal entrapment.

We have designed three fusogenic peptide sequences with a core amphiphilic sequence repeat to enable endosomal membrane fusion in response to the acidic endosomal environment, each attached to a poly-D-arginine tail to allow efficient complexing of peptides with siRNA cargo through electrostatic interactions.[23,45] We have shown that each DIV3(X) peptide variant can efficiently complex with

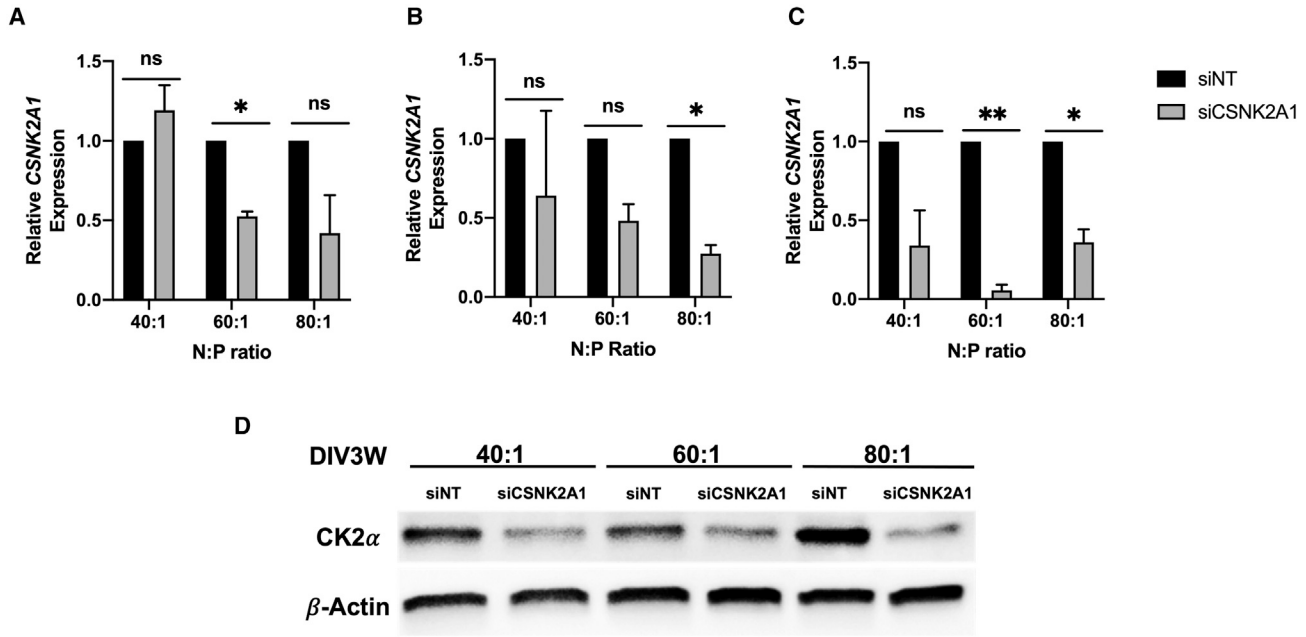

Figure 6. Fusogenic-mediated bioactivity of siRNAs in OVCAR3 cells

qPCR analysis of *CSNK2A1* mRNA after treatment of OVCAR3 cells with DIVA3 (A) DIV3H (B) and DIV3W (C) peptides complexed with siNT or siCSNK2A1 for 48 h. Data are mean ± SEM of three independent experiments analyzed with Student's t test within each N:P ratio. *$p \leq 0.05$; **$p \leq 0.01$; ns, not significant. (D) Western blot analysis of *CSNK2A1* protein product, CK2α, after treatment of OVCAR3 cells with DIV3W-siCSNK2A1 for 48 h β-Actin expression was monitored to ensure equal protein loading.

siRNAs, form monodisperse nanoparticles, and protect siRNAs from serum and RNase degradation, which are characteristics appropriate for systemic delivery and increased circulation time to allow for the accumulation of nanoparticles in the tumor microenvironment.

After characterizing the peptide/siRNA complexes, we examined the ability of the fusogenic peptides to mediate efficient delivery of siRNAs into ovarian cancer cells *in vitro*. DIV3W significantly outperformed DIVA3 and DIV3H in enhancing the internalization of siRNAs into OVCAR3 cells. We also observed that cellular internalization of siRNAs into ovarian cancer cells increased with increasing N:P ratio for each peptide due to greater hydrophobicity and positive charge. Increases in primary sequence hydrophobicity, and therefore, hydrophobicity of the supramolecular assembled complex, conferred by the tryptophan residue in DIV3W, may attribute to the increased internalization of siRNA by DIV3W compared with the DIVA3 and DIV3H peptides. Peptide sequences including tryptophan have previously been shown to increase cellular membrane affinity and endocytotic activity,[23,34,46] which was further validated in our studies with increased siRNA internalization mediated by DIV3W. The differences in endosomal entrapment and later escape in each peptide variation, determined by levels of gene knockdown, may be attributed to the increased affinity for pH-dependent conformation change and increased hydrophobicity with the addition of histidine and tryptophan amino acid residues, respectively.[16,36,46,47] Although peptide conformational change to helical secondary structure is required for α helix formation,[36] inclusion of the tryptophan residue in DIV3W inherently enables higher membrane affinity with increased hydrophobicity before pH changes occur, through the insertion of the hydrophobic R groups into the endosomal membrane.[46,47] Because of this, we suspect that DIV3W enhances endosomal escape and release of bioactive siRNA into the cytosol. Furthermore, viability studies demonstrated that DIV3(X) peptides did not cause cytotoxicity alone without siRNA cargo.

The selection of the optimal DIV3(X) peptide variant was confirmed through qPCR and western blot analysis of siRNA bioactivity. The bioactivity confirmed among all peptide variants also reflects the stability of the complexes in serum since all gene silencing experiments were conducted in the presence of serum to replicate physiologically relevant conditions. Compared with the other peptide variants, the enhanced siRNA bioactivity achieved with DIV3W aligns with previous assays, as DIV3W also demonstrated the highest siRNA protection and endosomal escape. These results demonstrate the potential of DIV3W as a delivery system for RNAi-based therapies and justify the selection of DIV3W as the fusogenic peptide for analysis of ovarian cancer cellular response to silencing the target gene.

CSNK2A1 has a vast array of roles in the activation of cellular pathways and processes. Many of these responses may be cancer-type-dependent; studies have shown that *CSNK2A1* activates phosphorylation of SIRT6 in breast cancer, the phosphoinositide 3-kinase (PI3K)-protein kinase B (Akt)-mammalian target of rapamycin (mTOR) pathway in gastric cancer, and nuclear factor κB (NF-κB)

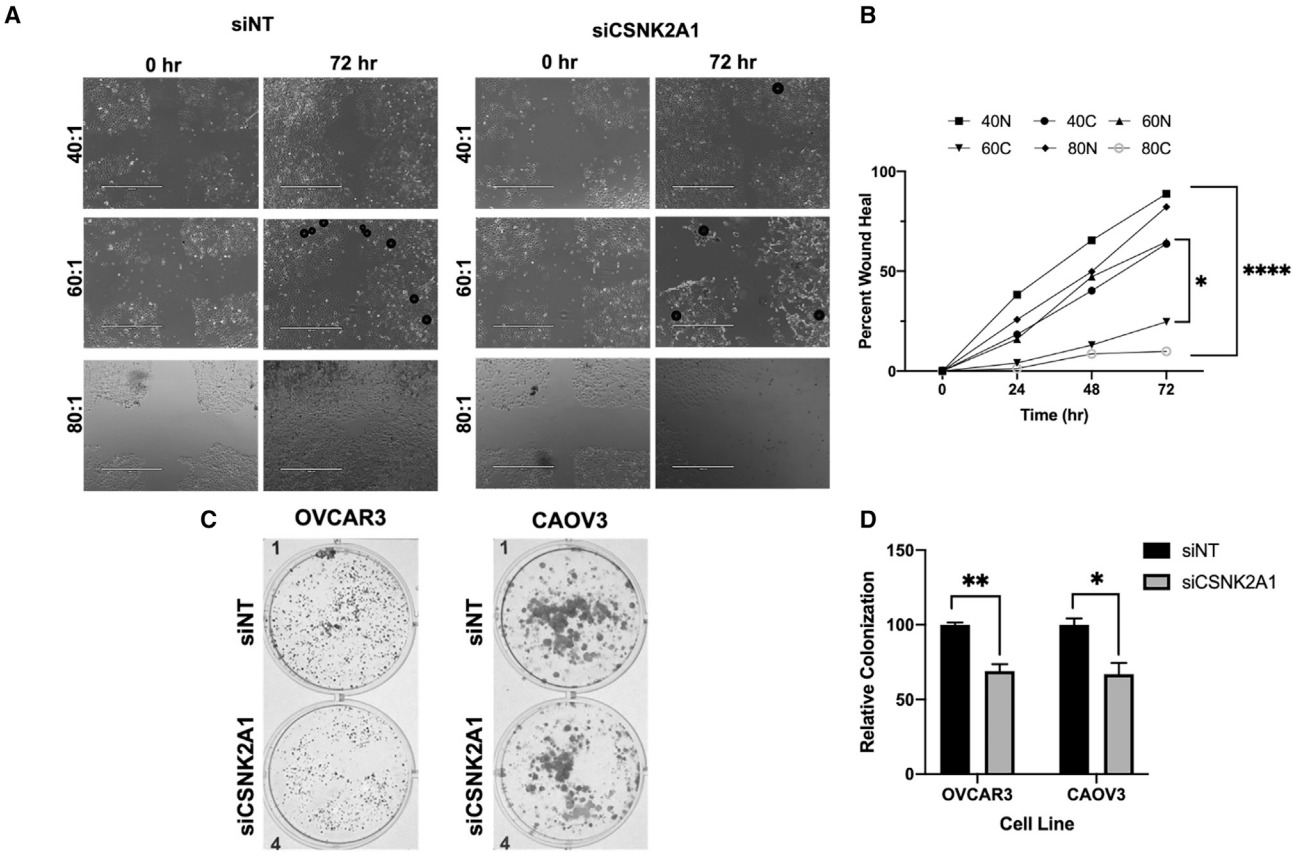

Figure 7. Downstream cellular effects of *CSNK2A1* knockdown

DIV3W complexed with (A) siNT or siCSNK2A1 at an 80:1 N:P ratio was delivered to OVCAR3 cells for 24 h and the ability of the cells to migrate across a scratch wound was observed using phase microscopy imaging over 72 h. Scale bar: 1,000 μm. (B) Cell regrowth over the course of 72 h was quantified with ImageJ and represented as percentage wound healing relative to the initial scratch distance. White-light imaging of clonogenic colony-forming assay of OVCAR3 (C) and CAOV3 cells 14 days after treatment with DIV3W-siCSNK2A1 at 80:1 N:P ratio. (D) The number of colonies was quantified and normalized to siNT negative control groups to assess recolonization. Data are mean ± SEM of three independent experiments and were analyzed using a two-way ANOVA with Tukey's multiple comparisons *post hoc* test and one-tailed T test for scratch and clonogenic results, respectively, where *$p \leq 0.05$, **$p \leq 0.01$, and ****$p < 0.0001$.

in glioblastoma, all contributing to poor patient prognosis.[48–50] In order to examine the effect of silencing *CSNK2A1* expression on oncogenic activity in ovarian cancer cells, viability, scratch migration, and colonization assays were completed after treatment with DIV3W-siCSNK2A1 complexes. While we did not observe any significant loss of cell viability after a 48-h treatment with DIV3W-siCSNK2A1 complexes, other studies have also demonstrated that knocking down *CSNK2A1* does not result in a loss in cell viability without including supplemental drug treatments due to the many roles of *CSNK2A1* in cell communication pathways in different cell types.[27,30,51,52] Silencing *CSNK2A1* did reduce cell migration, which is consistent with previous reports that show upregulated *CSNK2A1* expression contributes to increased cancer aggressiveness and decreased survivability rates in several cancer types.[48,51,53] Additionally, it has been demonstrated that *CSNK2A1* expression mediates the PI3K-Akt-mTOR pathway, attributing to increased oncogenesis, migration, and invasion.[49] Knockdown of *CSNK2A1* via lentiviral transfection in gastric cancer cells inhibited migration across a scratch wound compared with cells with high *CSNK2A1* expression.[49] It was also observed that *CSNK2A1* knockdown in gastric cancer cells reduced their invasion,[49] which, combined, may correlate to decreased cancer cell regrowth after treatment, reducing distant metastatic spread. Additionally, studies have shown that overexpression of *CSNK2A1* and its protein product, CK2α, enhance the clonogenic survivability of melanoma cells.[54] Our results are consistent with this observation; silencing of *CSNK2A1* mediated by the DIV3W peptide significantly reduced the clonogenicity of OVCAR3 and CAOV3 ovarian cancer cells. This consistency between cancer models also suggests that *CSNK2A1*'s roles in tumorigenesis can possibly be narrowed to cell communication, enhancing migration and regrowth.

To further evaluate the clinical translatability of the DIV3W peptide system as a gene delivery tool, we examined the peptide's ability to deliver bioactive siRNAs into ovarian tumor tissue using murine

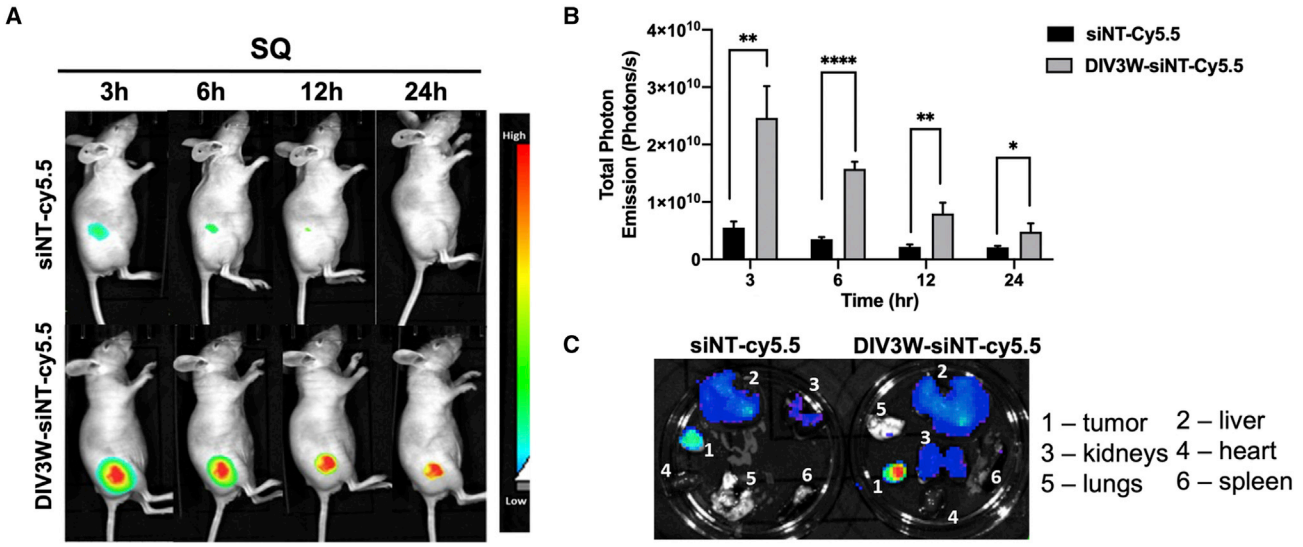

Figure 8. SQ delivery of DIV3W-siNT complexes in SQ flank ovarian tumor model

Naked siNT-Cy5.5 or DIV3W-siNT-Cy5.5 nanoparticles were delivered intratumorally to SQ tumors (A) and siRNA uptake was quantified from fluorescence using total photo emissions (B). (C) Mice were imaged at 3-, 6-, 12-, and 24-h intervals before euthanasia and *ex vivo* imaging. Quantification of total photon emission (photons/s) was completed with Aura software after normalization to siNT controls. Data are mean ± SEM of N = 3 and analyzed via two-way ANOVA with Tukey's multiple comparisons *post hoc* test, where *p ≤ 0.05, **p ≤ 0.01, and ****p ≤ 0.0001.

xenograft models. The cell line used in this study, OVCAR3, was selected because of its clinical relevance to high-grade serous ovarian adenocarcinoma in addition to its use in our *in vitro* work.[55,56] However, this cell line has had difficulty developing xenograft tumor models without using a supplementary basement matrix or delivering high quantities of cells.[56–58] To address this issue, we delivered OVCAR3 cells in a 50% v/v solution containing 10% Matrigel. While SQ tumors were successfully grown and easily

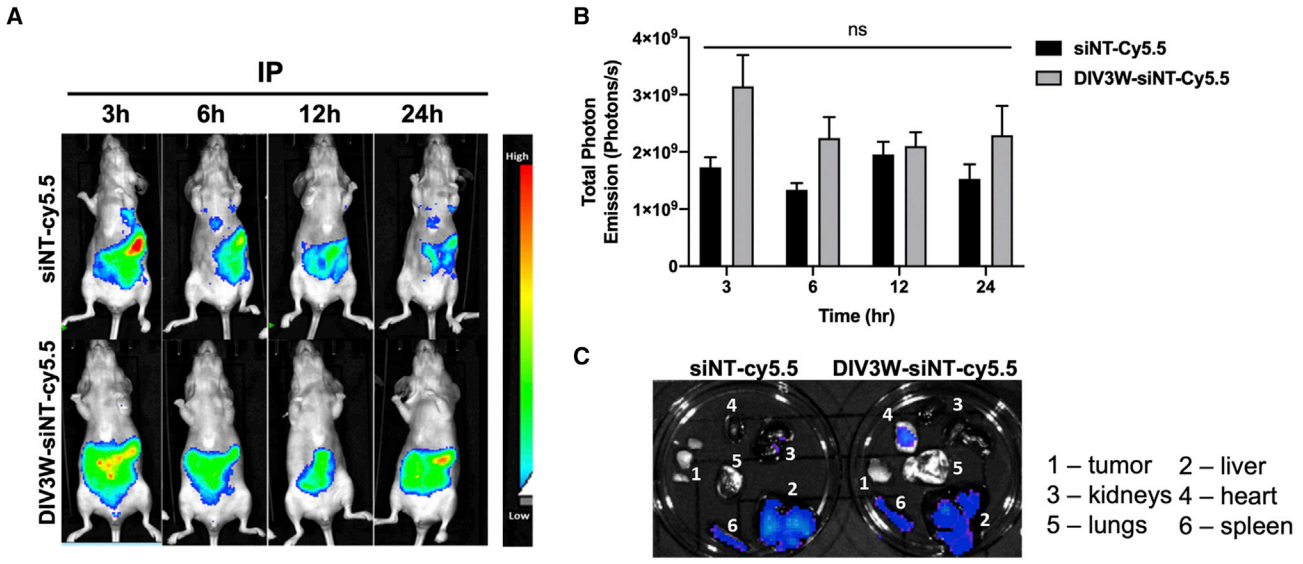

Figure 9. IP delivery of DIV3W-siNT complexes in IP ovarian tumor model

Naked siNT-Cy5.5 or DIV3W-siNT-Cy5.5 nanoparticles were delivered IP to IP tumors (A) and siRNA uptake was quantified from fluorescence using total photo emissions (B). (C) Mice were imaged at 3-, 6-, 12-, and 24-h intervals before euthanasia and *ex vivo* imaging. Quantification of total photon emission (photons/s) was completed with Aura software after normalization to siNT controls. Data are mean ± SEM of N = 3 and analyzed via two-way ANOVA with Tukey's multiple comparisons *post hoc* test. ns, not significant.

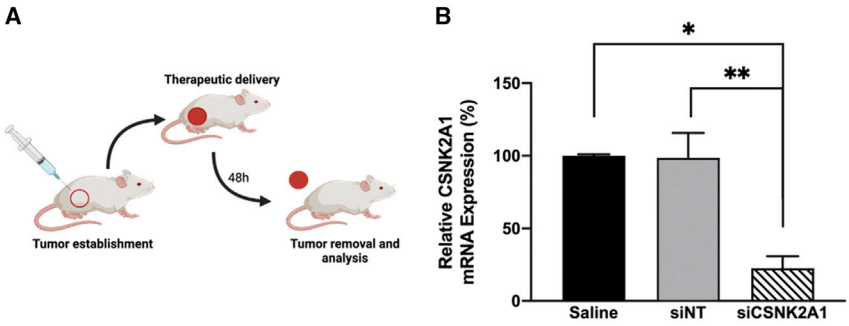

Figure 10. DIV3W-siCSNK2A1-mediated knockdown of *CSNK2A1* in SQ ovarian tumors 24 h post treatment

(A) Treatment procedure for SQ animal groups and (B) the resulting relative *CSNK2A1* expression for animals treated with saline (N = 2), DIV3W-siNT (N = 4), and DIV3W-siCSNK2A1 (N = 4) in SQ tumors. Data are mean ± SEM reported as relative *CSNK2A1* expression analyzed via one-way ANOVA with Tukey's multiple comparisons where *p ≤ 0.05 and **p ≤ 0.01 compared with saline and siNT controls.

observed, cells injected IP exhibited sporadic development of palpable tumors.

Following tumor establishment, we examined whether the DIV3W peptide delivered siRNAs into ovarian tumor tissue. Similar to other peptide-siRNA carriers delivered via intratumoral injection into SQ tumors in mice,[9,59] our results revealed that the novel fusogenic peptide enhanced retention of siRNA in tumor tissue via intratumoral delivery in SQ tumors, demonstrating the stability of the complex and potential to prevent siRNA degradation. We also observed siRNA signal in organs of the mononuclear phagocytic system when treatment was administered via both IP and intratumoral routes. However, accumulation of delivery systems in off-target sites, such as the kidney, liver, and spleen, is not uncommon, especially when delivered systemically.[60,61] We suspect that, because DIV3W is not functionalized with an active targeting component, this may contribute to nonspecific delivery. Several studies have incorporated an active targeting moiety to increase tumor targeting for peritoneal carcinomas and metastasis[62–64]; however, there have been conflicting results on whether a targeting component increases tumor targetability for IP delivery. Nonetheless, intratumoral administration of treatments into SQ tumors exhibited significant tumor uptake and warranted further investigation through bioactivity and anticancer studies.

We examined the ability of the DIV3W peptide to mediate delivery of bioactive siRNAs in a single-dose study where significant *CSNK2A1* mRNA knockdown provided the rationale for conducting a multi-dose study to assess the anticancer and downstream effects of targeting *CSNK2A1*. We noted an unexpected increase of *CSNK2A1* mRNA in tumors treated with the DIV3W-siNT control. Because there were no visual differences in the mice, increased mRNA expression could be due to off-target effects of the siNT. While our non-targeting siRNA has no known gene targets in mice or humans, it is possible that repeated treatment over 2 weeks affected *CSNK2A1* mRNA in a concentration-dependent manner, which has been reported elsewhere.[65] Our results indicate that this phenomenon could also be dose dependent since our single-dose bioactivity studies did not show an increase in *CSNK2A1* mRNA expression; however, this occurrence needs to be further evaluated. Silencing of *CSNK2A1* in ovarian tumor tissue mediated by DIV3W-siCSNK2A1 complexes led to several downstream effects. The significantly suppressed tumor growth coincides with the ability of siCSNK2A1 to reduce cell migration and invasion, as reported in our *in vitro* data. Because *CSNK2A1* is thought to play a role in migration, invasion, and the PI3K-Akt-mTOR pathway,[30,49] we sought to further explore its role in migration and proliferation by analyzing the expression of vimentin and Akt. The decreased expression of both genes indicates a reduction in migration and proliferation, providing further rationale for the reduced tumor growth observed when DIV3W-siCSNK2A1 was administered to SQ tumors in the multi-dosing study. These results provide additional insight into the relevance of *CSNK2A1* as a gene target in ovarian cancer.

Overall, this study demonstrates the ability of a series of fusogenic peptides composed of amphiphilic core repeats and a cationic poly-(D)-arginine tail to efficiently complex with, protect, and deliver therapeutic siRNA into ovarian cancer cells. The DIV3W peptide proved optimal for enhancing intracellular delivery, endosomal escape, and silencing of *CSNK2A1* mRNA and CK2α protein expression to reduce cellular migration and proliferation *in vitro* and *in vivo*. These results demonstrate the potential of the DIV3W peptide for the delivery of RNAi therapeutics and the potential of *CSNK2A1* as a therapeutic gene target to treat ovarian cancer.

MATERIALS AND METHODS

Cell culture

Ovarian epithelial cancer cell lines, OVCAR3, obtained from the American Type Culture Collection (ATCC, Manassas, VA), and CAOV3 (donated from Hollings Cancer Center, Charleston, SC) were cultured in McCoy's 5A culture medium and Dulbecco's modified Eagle's medium (DMEM, ATCC) respectively, supplemented with 10% fetal bovine serum (FBS, Corning, Corning, NY) and 1% penicillin/streptomycin (P/S) antibiotic solution (Corning). All cultures were incubated at 37°C in 5% CO_2.

Peptide synthesis

Peptides DIVA3 (WEADIVADIVADIVAGGG-(d)RRRRRRRRR), DIV3H (WEADIVADIVHDIVADIVAGGG-(d)RRRRRRRRR), and DIV3W (WEADIVADIVWDIVADIVAGGG-(d)RRRRRRRRR) were synthesized, purified (>95% purity), and analyzed via high-performance liquid chromatography (HPLC) by Genscript (Genscript USA, Piscataway, NJ). All formulations contained an end sequence

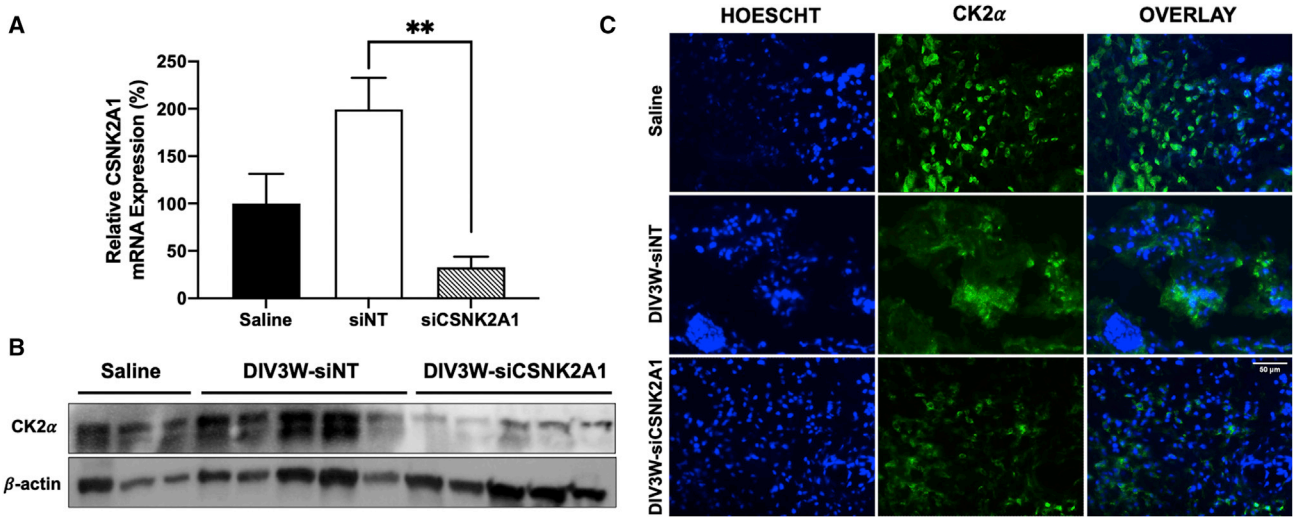

Figure 11. *CSNK2A1* mRNA and CK2α protein expression following a multi-dosing regimen of DIV3W-siCSNK2A1 in SQ ovarian tumors

(A) *CSNK2A1* gene expression quantified via qPCR relative to saline-treated controls. (B) Western blot analysis of CK2α knockdown caused by *CSNK2A1* gene silencing. (C) Immunocytochemistry of CK2α protein expression (GFP, green) in 0.5-μm tumor tissue sections with nuclei stained with Hoechst 33342 (blue). Data are mean ± SEM of N = 5 analyzed via one-way ANOVA, where $^{**}p < 0.01$. Scale bar: 50 μm.

of nine D-arginine residues with no terminal modifications. Lyophilized peptide formulations were resuspended in analytical-grade dimethyl sulfoxide (DMSO) to create stock peptide solutions of 100 μM (10 mg/mL). Working solutions of 10 μM (1 mg/mL) were created using a 1:10 dilution of stock peptide in RNase-free water, and all solutions were stored at −80°C.

Gel shift assays

DIVA3, DIV3H, and DIV3W (all three denoted as DIV3(X)) peptides resuspended in RNase-free water (10 μM) were thawed and kept on ice prior to complexation with 10 μM negative control siGENOME non-targeting siRNA #5 (siNT, GE Healthcare Dharmacon, Lafayette, CO) in RNase-free water and incubated for 20 min at room temperature to allow the formation of DIV3(X)-siNT complexes. Various molar ratios of peptides were complexed with siNT at increasing N:P molar ratios to determine the minimum molar ratio necessary to completely complex free siRNAs using an electrophoretic mobility shift assay. To determine the ability of each peptide variant to protect siRNAs from degradation, DIV3(X)-siNT complexes or siNT alone was left untreated or incubated with either 50% v/v FBS or 5 μg/mL RNase A at 37°C for 1 h. After this, complexes were dissociated using 6% sodium dodecyl sulfate (SDS). Samples were added to a 2% agarose gel and run at 100 V. Gels were stained with ethidium bromide, subsequently destained with Milli-Q water, and the gel was imaged using a ChemiDoc XRS imager (Bio-Rad, Hercules, CA).

Dynamic light scattering and TEM

DIV3(X)-siNT complexes were prepared at 2 mg/mL in RNase-free water as previously described. Hydrodynamic size and surface charge of the peptide/siRNA complexes were determined using a Nano ZS Zetasizer (Malvern Pananalytical, Malvern, UK). All data were recorded using Malvern's Zetasizer software.

In order to obtain TEM images of the peptide-siRNA complexes, DIV3W-siNT complexes were prepared as previously described to a concentration of 1 mg/mL in RNase-free water. After a 20-min incubation, TEM samples were prepared via drop casting onto a copper mesh grid. Following a 5-min drying period, the remaining water was wicked away, and the sample was background stained with 1% uranyl acetate solution (Electron Microscopy Sciences, Hatfield, PA). Samples were stored for 48 h to allow for complete solution evaporation and sample crystallization. TEM was completed using a Hitachi HT7800 microscope (Hitachi, White Plains, NY) and imaged at 80,000× magnification.

Cytotoxicity

Cells were seeded at 10,000 cells/well with complete culture medium in a 96-well plate and incubated overnight to allow the cells to attach. DIV3(X) peptides were complexed with siNT at 40:1-80:1 N:P molar ratios. DIV3(X)-siNT complexes were incubated with OVCAR3 or CAOV3 cells at a final concentration of 100 nM siRNA and 10% FBS for 24 h, after which medium was aspirated and cells were washed with 1× phosphate-buffered saline (PBS) and fresh medium with 10% FBS was added to each well and incubated for another 24 h.

Viability was measured using an MTS assay performed with CellTiter 96 AQueous One Solution Cell Proliferation Assay (Promega, Madison, WI). Assay reagent was added according to the manufacturer's protocol, and cells were incubated for 4 h. Absorbance was read using a BioTek Synergy LX (BioTek, Winooksi, VT) plate reader at 490 nm.

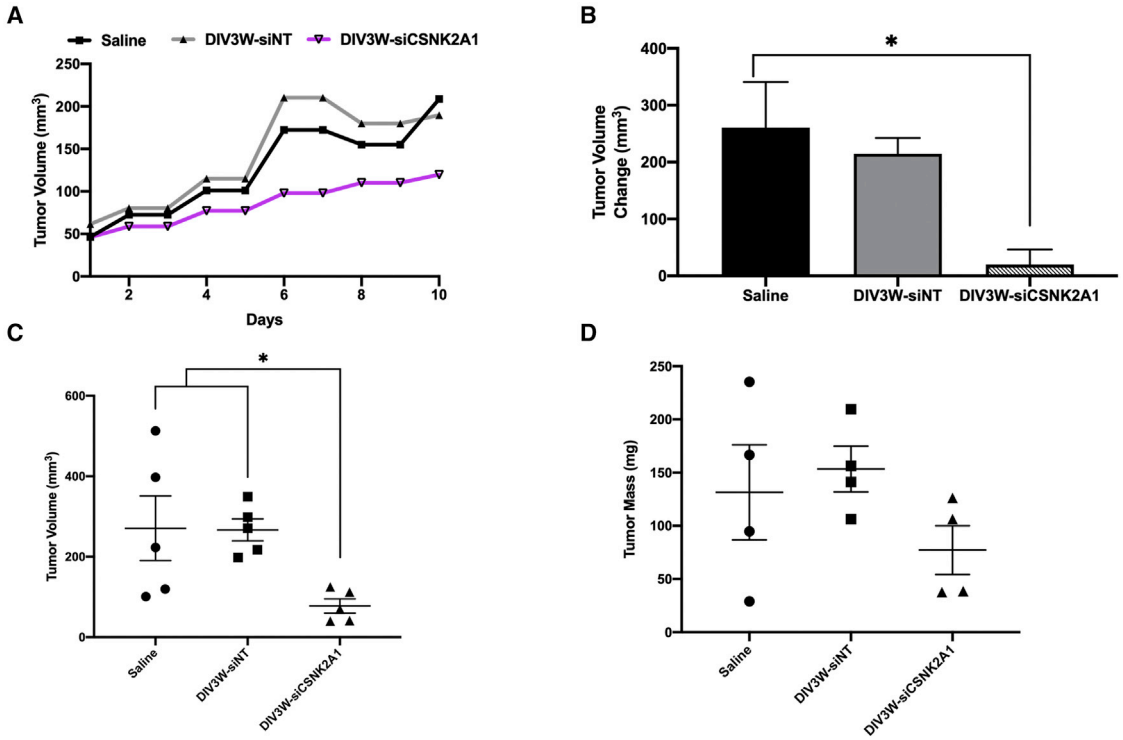

Figure 12. Evaluation of ovarian tumor growth following multi-dosing treatment with DIV3W-siCSNK2A1

(A) Tumor growth over time for saline, DIV3W-siNT, and DIV3W-siCSNK2A1-treated mice in the multi-dose schedule. (B) Tumor volume change from treatment injection 1 through final excised volume measurement. Tumor mass (C) and tumor volumes (D) recorded after euthanasia and tumor harvesting. Data are mean ± SEM of N = 5 and analyzed via one-way ANOVA, where *$p < 0.05$.

An MTS cell viability assay was also conducted as described for OVCAR3 and CAOV3 cells treated with DIV3W-siRNA complexes.

Cellular uptake

OVCAR3 and CAOV3 cells were prepared as previously described at 50,000 cells/well in a 24-well plate. DY547 fluorescently labeled siNT (siNT-DY547, GE Healthcare Dharmacon) was complexed with the DIV3(X) peptides in RNase-free water at 40:1 to 80:1 N:P molar ratios and incubated with OVCAR3 or CAOV3 cells for 4 h. Post incubation, medium was aspirated, and cells were washed with 1× PBS. To counterstain the nuclei, SuperSignal NucBlue Hoechst 33342 stain (Thermo Fisher Scientific, Waltham, MA) was added to the cells for 30 min, followed by an additional 1× PBS wash. Subsequent imaging was performed using an EVOS FL microscope (Thermo Fisher Scientific) at 10× magnification. For flow cytometric analysis, cells were detached, resuspended in 1× PBS, and analyzed using an Attune NXT Acoustic flow cytometer (Invitrogen, Carlsbad, CA) with the blue laser line and BL2 (574/26 nm) channel.

For analysis of endosomal escape, following the 4- and 8-h treatments, OVCAR3 and CAOV3 cells were fixed with 4% paraformaldehyde in 1× PBS and permeated with 0.5% Triton X-100 in 1× PBS for 15 min at room temperature. Blocking was completed after washing three times with 1× PBS by incubating with 1% BSA in 1× PBS for 30 min at room temperature. Primary antibodies for early endosome antigen-1 (rabbit anti-EEA1, Thermo Fisher) were diluted in 1× PBS (1:100) and incubated with cells for 1 h at 4°C in the dark. Following washing three times using 1× PBS, cells were incubated with Alexa Fluor 488 goat anti-rabbit secondary antibodies (Invitrogen) in a 1:100 dilution at room temperature for 1 h. Cells were washed three more times with 1× PBS, stained with SuperSignal NucBlue Hoechst 33342 (Thermo Fisher Scientific), and imaged using an EVOS FL microscope at 10× magnification.

qRT-PCR

Cells were seeded at 50,000 cells/well as previously described and treated with siRNA targeting *CSNK2A1* (siCSNK2A1 #s3638, Thermo Fisher Scientific) at increasing N:P ratios, as described previously, and incubated for a total of 48 h in McCoys 5A/DMEM-10% FBS. Treated cells were washed with 1× PBS at 24 h, and fresh medium was added. RNA isolation was completed using a Qiagen Mini-RNeasy Kit (Qiagen, Hilden, Germany) according to the manufacturer's protocol. RNA isolation quality and quantity were measured through the Gen5 protocol using a Take3 plate (BioTek). RNA was reverse transcribed using the QuantiTect Reverse Transcription kit (Qiagen). Real-time qPCR was completed with a QuantStudio 3 qPCR system (Applied Biosystems) using Applied Biosystems TaqMan FAST Master Mix (Thermo Fisher)

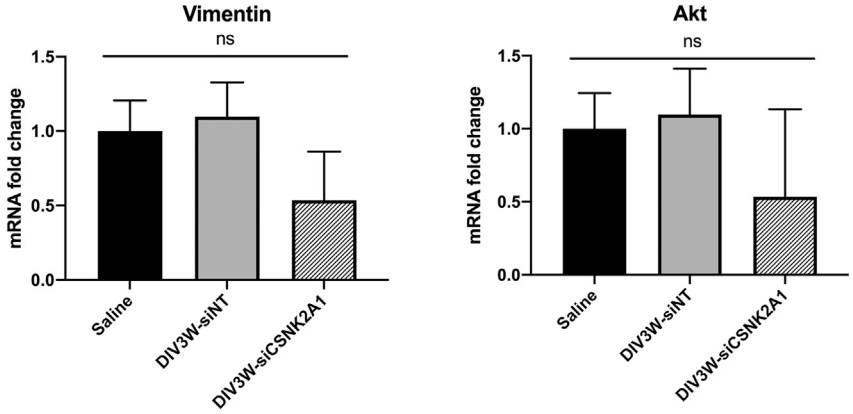

Figure 13. Vimentin and Akt mRNA expression following DIV3W-siCSNK2A1 multi-dose treatment in ovarian tumor

Vimentin and Akt mRNA expression fold change after multi-dosing treatment with DIV3W-siCSNK2A1 relative to the saline control. Data are mean ± SEM of N = 4 and analyzed via one-way ANOVA. ns, not significant.

and *CSNK2A1* (ID# Hs00751002_s1) and 18S (ID# Hs99999901_s1) predesigned TaqMan probes according to the manufacturer's protocol.

Western blot

Cells were seeded at 100,000 cells/well with complete culture medium in a six-well plate and left to incubate overnight. Cells were washed and treated with DIV3(X)-siRNA complexes as previously described. Following the 48-h treatment, cells were washed with 1× PBS and lysed with cold radioimmunoprecipitation assay (RIPA) buffer supplemented with protease inhibitor cocktail (Thermo Fisher). Protein concentrations were determined via bicinchoninic assay according to the manufacturer's protocol and absorbance was read at 562 nm. Equivalent protein concentrations for each treatment condition were separated by SDS-PAGE on a Bio-Rad Stain-Free 10% gel according to Bio-Rad protocols and transferred to a stain-free PVDF membrane using a wet transfer system. The PVDF membrane was cut at appropriate molecular weight intervals consistent with protein weights analyzed and blocked for 1 h with 5% non-fat dried milk solution in 1× Tris-HCl-buffered saline 0.1% Tween 20 (TBST) at room temperature. Blots were probed at 4°C overnight with rabbit monoclonal anti-CK2α antibody (1:1,000, Invitrogen) or mouse monoclonal anti-β-actin (1:10,000, Sigma-Aldrich, St. Louis, MO). Membranes were washed five times with 1× TBST and incubated with goat anti-rabbit (1:1,000, Thermo Fisher) or goat anti-mouse (1:10,000, Thermo Fisher) secondary antibodies for 1 h at room temperature. Five additional washes with 1× TBST were performed, and protein bands were detected with SuperSignal West Pico Plus Chemiluminescent Substrate (Thermo Fisher) and imaged using a Bio-Rad ChemiDoc Imaging System.

Cell migration and colonization analysis

Scratch migration was completed by seeding OVCAR3 or CAOV3 cells at 100,000 cells/well in a 12-well plate to achieve near 100% confluency. Following a 48-h treatment with DIV3W-siCSNK2A1 or DIV3W-siNT complexes, a vertical and horizontal scratch was made in the cell monolayer using a 200-μL micropipette tip, and edges were smoothed using a gentle wash with 1× PBS. Cells were imaged with an EVOS FL microscope at 4× magnification at 24-h intervals at the cross intersections to ensure consistent imaging areas. Using image analysis software, measurements across the horizontal axis were taken for each image, with wound closure percentages calculated at each time point using the equation below (Equation 1) where t_i is the distance at any time point i and t_0 is the distance at time 0.

$$Percent\ Wound\ Heal\ (t_i) = 100 - \left[\frac{(t_i - t_0)}{t_0} \times 100\right]\% \quad \text{(Equation 1)}$$

In the formula for calculating percentage wound heal in the scratch wound assay, the distance at t = *0*, t_0, was deducted from each subsequent distance measurement, t_i, at t = *i*. Distance difference was normalized to t_0 and subtracted from 100 to represent the percentage distance closed from t_0.

Colonization of treated cells was determined using a clonogenic assay and quantified via absorbance at 490 nm. Cells were seeded at 50,000 cells/well in a 24-well plate and treated with DIV3W- siCSNK2A1 or DIV3W-siNT complexes as previously described. Cells were harvested, counted, and reseeded in a six-well plate at a concentration of 2,500 cells/well. Cell growth was monitored for 14 days with medium changes every 2 days. After the growth period, cells were washed with 1× PBS and stained with a 0.1% crystal violet solution for 30 min. Unbound crystal violet was washed with double-distilledH_2O (ddH_2O), and plates were air-dried for 15 min and imaged with the ChemiDoc Imaging System. Recolonization was quantified by manual counting of colonies formed, and data were normalized to siNT-treated groups.

Generation of tumor xenografts

All mouse procedures and experiments were approved by the Clemson University Institutional Animal Care and Use Committee (IACUC) and completed in accordance with the Guide for the Care and Use of Laboratory Animals (NIH) and Godley-Snell Animal Research Facility (GSRC) Animal Use policies. Procedures for generating xenograft SQ and IP ovarian cancer tumors were derived and modified from previous works.[9,26,27] Athymic nude-FoxN1^{nu} mice were obtained at 6–7 weeks of age (Envigo, Indianapolis, IN). OVCAR3 cells were cultured and grown to 50% confluence as described previously, harvested, and 10 × 10^6 cells were suspended

in 100 μL of 10% Matrigel matrix suspension (Corning, Corning, NY) in 1:1 ratio (v/v) of medium/Matrigel. Cell suspensions were injected into mice either SQ in the right flank or IP into the lower right quadrant. Tumors were grown for 14 days before administration of treatment.

In vivo and *ex vivo* imaging

After tumor growth was established and tumors measured at least 50 mm^3, siNT-Cy5.5 alone or DIV3W-siNT-Cy5.5 complexes at an siRNA dosage of 0.5 mg/kg were delivered intratumorally to SQ tumors or IP to IP tumors. Animals were imaged 3, 6, 12, and 24 h post treatment using the PerkinElmer IVIS Spectrum In Vivo Imaging System (PerkinElmer, Waltham, MA). Gray-scale images were obtained using 2 × 2 binning and fluorescent images were captured using the Cy5 optical filter, also using 2 × 2 binning. Images were acquired and formatted to inverted rainbow spectrum using LivingImage software (PerkinElmer) and exported for fluorescence intensity quantification using Aura software (Spectral Instruments, Tucson, AZ). After 24 h, animals were euthanized according to IACUC and GSRC protocols, and tumor, heart, lungs, liver, kidneys, and spleen were explanted for *ex vivo* imaging with quantification as described.

qPCR and western blot analysis

SQ and IP tumors were treated with saline, DIV3W-siNT, or DIV3W-siCSNK2A1 for either 48 h or in a multi-dose schedule over 2 weeks. Mice were injected with 0.5 mg/kg of siRNA at each treatment, and multi-dosing occurred every 3 days for four doses. Tumors were measured in two dimensions using digital calipers, and tumor volumes were calculated using the formula: $d^2 \times D/2$, where d is the smaller dimension.[18] Mice were euthanized 48 h post injection of the final dose. Tumors were resected after euthanasia and stored in RNAlater at 4°C (Thermo Fisher). Tumor tissue was then homogenized, and the lysate was processed using a Qiagen AllPrep RNA/Protein kit (Qiagen, Hilden, Germany). RNA isolation was performed according to Qiagen protocols and was quantified using a Take3 plate (BioTek, Winooksi, VT) and the Gen5 analysis software. RNA was reverse transcribed using the QuantiTect Reverse Transcription kit (Qiagen). Real-time qPCR was completed with a QuantStudio 3 qPCR system (Applied Biosystems) using Applied Biosystems TaqMan FAST Master Mix (Thermo Fisher) and *CSNK2A1* (ID# Hs00751002_s1), *AKT1* (ID#Hs00178298_m1), *VMAC* (ID#Hs00418522_m1), and *18S* (ID# Hs99999901_s1) predesigned TaqMan probes according to the manufacturer's protocol. For protein measurement via western blot, lysates were processed using the Qiagen AllPrep RNA/Protein kit (Qiagen), and total protein was quantified via bicinchoninic assay according to the manufacturer's protocol.

Immunocytochemistry

SQ and IP tumor fragments from the multi-dose anticancer study were snap-frozen using liquid nitrogen and embedded in Scigen Tissue-Plus OCT Compound (Thermo Fisher Scientific). Samples were sectioned on a cryostat to approximately 10-μm depths and mounted on histological slides. Tissue samples were incubated with cold blocking buffer containing 1% BSA in 1× PBS for 30 min at room temperature, washed with cold 1× PBS twice, and incubated with anti-CK2α antibody (1:100, Invitrogen) overnight at 4°C. Samples were then washed with cold 1× PBS and incubated with Alexa Fluor 488 goat anti-mouse antibody (Thermo Fisher Scientific) for 1 h. Tissue samples were washed three times with cold 1× PBS, incubated with SuperSignal NucBlue Hoechst 33342 (Thermo Fisher Scientific) for 20 min, and washed three more times with 1× PBS prior to imaging. Images were acquired using an EVOS FL microscope.

Statistical analysis

All data are mean ± SEM of three independent experiments. Statistical comparisons were carried out using GraphPad Prism 8.4.3. Comparisons between two independent groups were conducted using a Student's t test. *In vivo* data were acquired to N = 3 in biodistribution studies, N = 4 in single-dose bioactivity studies, and N = 5 in multi-dose anticancer studies for all experimental groups. Saline controls were acquired to N = 2 in bioactivity experiments. Three or more independent groups with one factor were analyzed using ANOVA and *post hoc* Tukey comparisons, and three or more independent groups with two factors were analyzed using two-way ANOVA, also with *post hoc* Tukey comparisons. Results were considered statistically significant where $p \leq 0.05$.

DATA AVAILABILITY

This study did not generate/analyze datasets or code.

SUPPLEMENTAL INFORMATION

Supplemental information can be found online at https://doi.org/10.1016/j.omtn.2022.09.012.

ACKNOWLEDGMENTS

This work was supported by the National Science Foundation EPSCoR program under NSF Award #OIA-1655740 (A.A.-B.) and the National Science Foundation Faculty Early Career Development Program under NSF Award #204669 (A.A.-B.). This work is also supported in-part by the Hollings Cancer Center Lowvelo Doctoral Fellowship Program (T.S.) and Clemson's Call Me Doctor Fellowship (K.L.A). Any opinions, findings, and conclusions or recommendations expressed in this material are those of the authors and do not necessarily reflect those of the National Science Foundation or the Hollings Cancer Center. We would like to thank all undergraduate members of our lab that assisted in cell culture as well as A. Simionescu, W. Richardson, R. Latour, N. Vyavahare, and G. Korneva for their generosity in allowing us to utilize the ChemiDoc Imaging System, EVOS FL Auto, and Attune NxT Flow Cytometer, which contributed to the production of data. We also thank J. Larsen in the Department of Chemical and Biomolecular Engineering at Clemson for the use of the Malvern Nano ZS Zetasizer. Special thanks to J. Delaney at the Medical University of South Carolina Department of Biochemistry and Molecular Biology for providing CAOV3 cells. Thank you to B. Booth for providing MCF10A cells. Additionally, figures were made using biorender.com.

AUTHOR CONTRIBUTIONS

T.S. and A.A.-B., conceptualization, methodology, validation, resources, and funding acquisition; T.S. and K.L.A., formal analysis, data curation, writing – original draft, visualization, and project administration; A.A.-B., writing – review & editing, and supervision; T.S., K.L.A., J.B., A.H., and S.G., investigation, and writing – review & editing.

DECLARATION OF INTERESTS

The authors declare no competing interests.

REFERENCES

1. Siegel, R.L., Miller, K.D., Fuchs, H.E., and Jemal, A. (2021). Cancer statistics, 2021. CA. Cancer J. Clin. *71*, 7–33.
2. Srivastava, S.K., Ahmad, A., Miree, O., Patel, G.K., Singh, S., Rocconi, R.P., and Singh, A.P. (2017). Racial health disparities in ovarian cancer: not just black and white. J. Ovarian Res. *10*, 58.
3. National Cancer Institute, and DCCPS Surveillance, Epidemiology, and End Results (SEER) Program. Research Data (1975-2019). National Cancer Institute.
4. Grunewald, T., and Ledermann, J.A. (2017). Targeted therapies for ovarian cancer. Best Pract. Res. Clin. Obstet. Gynaecol. *41*, 139–152.
5. Champer, M., Huang, Y., Hou, J.Y., Tergas, A.I., Burke, W.M., Hillyer, G.C., Ananth, C.V., Neugut, A.I., Hershman, D.L., and Wright, J.D. (2018). Adherence to treatment recommendations and outcomes for women with ovarian cancer at first recurrence. Gynecol. Oncol. *148*, 19–27.
6. Alexander-Bryant, A.A., Zhang, H., Attaway, C.C., Pugh, W., Eggart, L., Sansevere, R.M., Andino, L.M., Dinh, L., Cantini, L.P., and Jakymiw, A. (2017). Dual peptide-mediated targeted delivery of bioactive siRNAs to oral cancer cells in vivo. Oral Oncol. *72*, 123–131.
7. Qin, B., Chen, Z., Jin, W., and Cheng, K. (2013). Development of cholesteryl peptide micelles for siRNA delivery. J. Control. Release *172*, 159–168.
8. Karagiannis, E.D., Alabi, C.A., and Anderson, D.G. (2012). Rationally designed tumor-penetrating nanocomplexes. ACS Nano *6*, 8484–8487.
9. Kim, S.W., Kim, N.Y., Choi, Y.B., Park, S.H., Yang, J.M., and Shin, S. (2010). RNA interference in vitro and in vivo using an arginine peptide/siRNA complex system. J. Control. Release *143*, 335–343.
10. Kim, D.H., and Rossi, J.J. (2007). Strategies for silencing human disease using RNA interference. Nat. Rev. Genet. *8*, 173–184.
11. Ozcan, G., Ozpolat, B., Coleman, R.L., Sood, A.K., and Medicine, R. (2016). Preclinical and clinical development of siRNA therapeutics. Adv. Drug Deliv. Rev. *87*, 108–119.
12. Alexander-Bryant, A.A., Berg-Foels, W.V., and Wen, X. (2013). Bioengineering strategies for designing targeted cancer therapies. Adv. Cancer Res. *118*, 1–53.
13. Goldberg, M.S. (2013). SiRNA delivery for the treatment of ovarian cancer. Methods *63*, 95–100.
14. Lehto, T., Ezzat, K., Wood, M.J.A., and El Andaloussi, S. (2016). Peptides for nucleic acid delivery. Adv. Drug Deliv. Rev. *106*, 172–182.
15. Tai, W., and Gao, X. (2017). Functional peptides for siRNA delivery. Adv. Drug Deliv. Rev. *110–111*, 157–168.
16. Erazo-oliveras, A., Muthukrishnan, N., Baker, R., Wang, T.Y., and Pellois, J.P. (2012). Improving the endosomal escape of cell-penetrating peptides and their cargos : strategies and challenges. Pharmaceuticals *5*, 1177–1209.
17. Oliveira, S., van Rooy, I., Kranenburg, O., Storm, G., and Schiffelers, R.M. (2007). Fusogenic peptides enhance endosomal escape improving siRNA-induced silencing of oncogenes. Int. J. Pharm. *331*, 211–214.
18. Nishimura, Y., Takeda, K., Ezawa, R., Ishii, J., Ogino, C., and Kondo, A. (2014). A display of pH-sensitive fusogenic GALA peptide facilitates endosomal escape from a Bio-nanocapsule via an endocytic uptake pathway. J. Nanobiotechnol. *12*, 11.
19. Cummings, J.C., Zhang, H., and Jakymiw, A. (2019). Peptide carriers to the rescue: overcoming the barriers to siRNA delivery for cancer treatment. Transl. Res. *214*, 92–104.
20. Samec, T., Boulos, J., Gilmore, S., Hazelton, A., and Alexander-Bryant, A. (2022). Peptide-based delivery of therapeutics in cancer treatment. Mater. Today. Bio *14*, 100248.
21. Cantini, L., Attaway, C.C., Butler, B., Andino, L.M., Sokolosky, M.L., and Jakymiw, A. (2013). Fusogenic-Oligoarginine peptide-mediated delivery of siRNAs targeting the CIP2A oncogene into oral cancer cells. PLoS One *8*, e73348.
22. Burks, S.R., Legenzov, E.A., Martin, E.W., Li, C., Lu, W., and Kao, J.P.Y. (2015). Co-encapsulating the fusogenic peptide INF7 and molecular imaging probes in liposomes increases intracellular signal and probe retention. PLoS One *10*, e0120982.
23. Subbarao, N.K., Parente, R.A., Szoka, F.C., Nadasdi, L., and Pongracz, K. (1987). pH-dependent bilayer destabilization by an amphipathic peptide. Biochemistry *26*, 2964–2972.
24. Alexander-Bryant, A.A., Dumitriu, A., Attaway, C.C., Yu, H., and Jakymiw, A. (2015). Fusogenic-oligoarginine peptide-mediated silencing of the CIP2A oncogene suppresses oral cancer tumor growth in vivo. J. Control. Release *218*, 72–81.
25. Sackett, K., and Shai, Y. (2005). The HIV fusion peptide adopts intermolecular parallel β-sheet structure in membranes when stabilized by the adjacent N-terminal heptad repeat: a 13C FTIR study. J. Mol. Biol. *350*, 790–805.
26. Domcke, S., Sinha, R., Levine, D.A., Sander, C., and Schultz, N. (2013). Evaluating cell lines as tumour models by comparison of genomic profiles. Nat. Commun. *4*, 2126.
27. Rabalski, A.J., Gyenis, L., and Litchfield, D.W. (2016). Molecular pathways: emergence of protein kinase CK2 (CSNK2) as a potential target to inhibit survival and DNA damage response and repair pathways in cancer cells. Clin. Cancer Res. *22*, 2840–2847.
28. Ma, Z., Wang, X., He, J., Xia, J., and Li, Y. (2017). Increased expression of protein kinase CK2α correlates with poor patient prognosis in epithelial ovarian cancer. PLoS One *12*, e0174037.
29. Litchfield, D.W. (2003). Protein kinase CK2: structure, regulation and role in cellular decisions of life and death. Biochem. J. *369*, 1–15.
30. Chua, M.M.J., Ortega, C.E., Sheikh, A., Lee, M., Abdul-Rassoul, H., Hartshorn, K.L., and Dominguez, I. (2017). CK2 in cancer: cellular and biochemical mechanisms and potential therapeutic target. Pharmaceuticals *10*, E18.
31. Pathak, H.B., Zhou, Y., Sethi, G., Hirst, J., Schilder, R.J., Golemis, E.A., and Godwin, A.K. (2015). A synthetic lethality screen using a focused siRNA library to identify sensitizers to dasatinib therapy for the treatment of epithelial ovarian cancer. PLoS One *10*, e0144126.
32. Siddiqui-Jain, A., Bliesath, J., Macalino, D., Omori, M., Huser, N., Streiner, N., Ho, C.B., Anderes, K., Proffitt, C., O'Brien, S.E., et al. (2012). CK2 inhibitor CX-4945 suppresses DNA repair response triggered by DNA-targeted anticancer drugs and augments efficacy: mechanistic rationale for drug combination therapy. Mol. Cancer Ther. *11*, 994–1005.
33. Li, W., Nicol, F., and Szoka, F.C. (2004). GALA: a designed synthetic pH-responsive amphipathic peptide with applications in drug and gene delivery. Adv. Drug Deliv. Rev. *56*, 967–985.
34. Sánchez-García, L., Serna, N., Mattanovich, M., Cazzanelli, P., Sánchez-Chardi, A., Conchillo-Solé, O., Cortés, F., Daura, X., Unzueta, U., Mangues, R., et al. (2017). The fusogenic peptide HA2 impairs selectivity of CXCR4-targeted protein nanoparticles. Chem. Commun. *53*, 4565–4568.
35. Thomas, O.S., and Weber, W. (2019). Overcoming physiological barriers to nanoparticle delivery—are we there yet? Front. Bioeng. Biotechnol. *7*, 415.
36. Hou, K.K., Pan, H., Schlesinger, P.H., and Wickline, S.A. (2015). A role for peptides in overcoming endosomal entrapment in siRNA delivery – a focus on melittin. Biotechnol. Adv. *33*, 931–940.
37. He, C., Liu, D., and Lin, W. (2015). Self-assembled nanoscale coordination polymers carrying siRNAs and cisplatin for effective treatment of resistant ovarian cancer. Biomaterials *36*, 124–133.
38. Roberts, C.M., Shahin, S.A., Wen, W., Finlay, J.B., Dong, J., Wang, R., Dellinger, T.H., Zink, J.I., Tamanoi, F., and Glackin, C.A. (2017). Nanoparticle delivery of siRNA

against TWIST to reduce drug resistance and tumor growth in ovarian cancer models. Nanomedicine. *13*, 965–976.

39. Leng, Q., Woodle, M.C., Lu, P.Y., and Mixson, A.J. (2009). Advances in systemic siRNA delivery. Drugs Future *34*, 721–737.
40. Kanekura, K., Harada, Y., Fujimoto, M., Yagi, T., Hayamizu, Y., Nagaoka, K., and Kuroda, M. (2018). Characterization of membrane penetration and cytotoxicity of C9orf72-encoding arginine-rich dipeptides. Sci. Rep. *8*, 12740.
41. Pei, D., and Buyanova, M. (2019). Overcoming endosomal entrapment in drug delivery. Bioconjug. Chem. *30*, 273–283.
42. Meng, Z., Luan, L., Kang, Z., Feng, S., Meng, Q., and Liu, K. (2017). Histidine-enriched multifunctional peptide vectors with enhanced cellular uptake and endosomal escape for gene delivery. J. Mater. Chem. B *5*, 74–84.
43. Midoux, P., and Monsigny, M. (1999). Efficient gene transfer by histidylated polylysine/pDNA complexes. Bioconjug. Chem. *10*, 406–411.
44. Kumar, V.V., Pichon, C., Refregiers, M., Guerin, B., Midoux, P., and Chaudhuri, A. (2003). Single histidine residue in head-group region is sufficient to impart remarkable gene transfection properties to cationic lipids: evidence for histidine-mediated membrane fusion at acidic pH. Gene Ther. *10*, 1206–1215.
45. Evans, J.C., Malhotra, M., Sweeney, K., Darcy, R., Nelson, C.C., Hollier, B.G., and O'Driscoll, C.M. (2017). Folate-targeted amphiphilic cyclodextrin nanoparticles incorporating a fusogenic peptide deliver therapeutic siRNA and inhibit the invasive capacity of 3D prostate cancer tumours. Int. J. Pharm. *532*, 511–518.
46. Christiaens, B., Symoens, S., Verheyden, S., Engelborghs, Y., Joliot, A., Prochiantz, A., Vandekerckhove, J., Rosseneu, M., Vanloo, B., and Vanderheyden, S. (2002). Tryptophan fluorescence study of the interaction of penetratin peptides with model membranes. Eur. J. Biochem. *269*, 2918–2926.
47. Lönn, P., Kacsinta, A.D., Cui, X., Hamil, A.S., Kaulich, M., Gogoi, K., and Dowdy, S.F. (2016). Enhancing endosomal escape for intracellular delivery of macromolecular biologic therapeutics. Sci. Rep. https://doi.org/10.1038/srep32301.
48. Bae, J.S., Park, S.H., Jamiyandorj, U., Kim, K.M., Noh, S.J., Kim, J.R., Park, H.J., Kwon, K.S., Jung, S.H., Park, H.S., et al. (2016). CK2α/CSNK2A1 phosphorylates SIRT6 and is involved in the progression of breast carcinoma and predicts shorter survival of diagnosed patients. Am. J. Pathol. *186*, 3297–3315.
49. Jiang, C., Ma, Z., Zhang, G., Yang, X., Du, Q., and Wang, W. (2019). Csnk2a1 promotes gastric cancer invasion through the pi3k-akt-mtor signaling pathway. Cancer Manag. Res. *11*, 10135–10143.
50. Dubois, N., Willems, M., Nguyen-Khac, M.T., Kroonen, J., Goffart, N., Deprez, M., Bours, V., and Robe, P.A. (2016). Constitutive activation of casein kinase 2 in glioblastomas: absence of class restriction and broad therapeutic potential. Int. J. Oncol. *48*, 2445–2452.
51. Sharma, A.L., Meitei, P.M., and Singh, N.T. (2019). Ovarian cancer G protein-coupled receptor 1 inhib- its A549 cells Migration through Casein kinase 2 α intronless gene and Neutral endopeptidase. BMC Cancer *22*, 143.
52. Bae, J.S., Park, S.H., Kim, K.M., Kwon, K.S., Kim, C.Y., Lee, H.K., Park, B.H., Park, H.S., Lee, H., Moon, W.S., et al. (2015). CK2α phosphorylates DBC1 and is involved in the progression of gastric carcinoma and predicts poor survival of gastric carcinoma patients. Int. J. Cancer *136*, 797–809.
53. Ortega, C.E., Seidner, Y., and Dominguez, I. (2014). Mining CK2 in cancer. PLoS One *9*, e115609.
54. Zhou, B., Ritt, D.A., Morrison, D.K., Der, C.J., and Cox, A.D. (2016). Protein kinase CK2α maintains extracellular signal-regulated kinase (ERK) activity in a CK2α kinase-independent manner to promote resistance to inhibitors of RAF and MEK but not ERK in BRAF mutant melanoma. J. Biol. Chem. *291*, 17804–17815.
55. Marcotte, R., Brown, K.R., Suarez, F., Sayad, A., Karamboulas, K., Krzyzanowski, P.M., Sircoulomb, F., Medrano, M., Fedyshyn, Y., Koh, J.L.Y., et al. (2012). Essential gene profiles in breast, pancreatic, and ovarian cancer cells. Cancer Discov. *2*, 172–189.
56. Beaufort, C.M., Helmijr, J.C.A., Piskorz, A.M., Hoogstraat, M., Ruigrok-Ritstier, K., Besselink, N., Murtaza, M., van IJcken, W.F.J., Heine, A.A.J., Smid, M., et al. (2014). Ovarian cancer cell line panel (OCCP): clinical importance of in vitro morphological subtypes. PLoS One *9*, e103988.
57. Tudrej, P., Kujawa, K.A., Cortez, A.J., and Lisowska, K.M. (2019). Characteristics of in vivo model systems for ovarian cancer studies. Diagnostics *9*, 120.
58. Hernandez, L., Kim, M.K., Lyle, L.T., Bunch, K.P., House, C.D., Ning, F., Noonan, A.M., Annunziata, C.M., Branch, M., Reed, W., et al. (2016). Characterization of ovarian cancer cell lines as in vivo models for preclinical studies. Gynecol. Oncol. *142*, 332–340.
59. Ryu, Y.C., Kim, K.A., Kim, B.C., Wang, H.M.D., and Hwang, B.H. (2021). Novel fusion peptide-mediated siRNA delivery using self-assembled nanocomplex. J. Nanobiotechnol. *19*, 44.
60. Liu, X., Wang, W., Samarsky, D., Liu, L., Xu, Q., Zhang, W., Zhu, G., Wu, P., Zuo, X., Deng, H., et al. (2014). Tumor-targeted in vivo gene silencing via systemic delivery of cRGD-conjugated siRNA. Nucleic Acids Res. *42*, 11805–11817.
61. Huang, Y., Wang, X., Huang, W., Cheng, Q., Zheng, S., Guo, S., Cao, H., Liang, X.J., Du, Q., and Liang, Z. (2015). Systemic administration of siRNA via cRGD-containing peptide. Sci. Rep. *5*, 12458.
62. Ikemoto, H., Lingasamy, P., Willmore, A.A., and Hunt, H. (2017). Hyaluronan-binding peptide for targeting peritoneal carcinomatosis. Tumour Biol. *39*. 1010428317701628.
63. Simón-Gracia, L., Hunt, H., and Teesalu, T. (2018). Peritoneal carcinomatosis targeting with tumor homing peptides. Molecules *23*, E1190.
64. Hunt, H., Simón-Gracia, L., Tobi, A., Kotamraju, V.R., Sharma, S., Nigul, M., Sugahara, K.N., Ruoslahti, E., and Teesalu, T. (2017). Targeting of p32 in peritoneal carcinomatosis with intraperitoneal linTT1 peptide-guided pro-apoptotic nanoparticles. J. Control. Release *260*, 142–153.
65. Persengiev, S.P., Zhu, X., and Green, M.R. (2004). Nonspecific, concentration-dependent stimulation and repression of mammalian gene expression by small interfering RNAs (siRNAs). RNA *10*, 12–18.